Journal of the Meteorological Society of Japan

The DOI for this manuscript is
DOI:10.2151/jmsj.2022-038
J-STAGE Advance published date: May 25th, 2022
The final manuscript after publication will replace the preliminary version at the above DOI once it is available.

The influences of Monsoon Trough on the relative motion of binary tropical cyclones

Han Li[1], Xuyang Ge[1*], Melinda Peng[2], Lu Li[3]

[1]Key Laboratory of Meteorological Disaster of Ministry of Education, Joint International Research Laboratory of Climate and Environment Change, Collaborative Innovation Center on Forecast and Evaluation of Meteorological Disasters, Nanjing University of Information Science and Technology, Nanjing 210044, China

[2]University of Colorado, Colorado Spring, Colorado

[3]Changde Meteorology Bureau, Hunan

May 16, 2022

Corresponding author: Xuyang Ge, NUIST, Email: xuyang@nuist.edu.cn

Abstract

In this study, the effect of the zonally-elongating monsoon trough (MT) on the binary tropical-cyclones (TCs) interaction is investigated by using data analysis and idealized simulations. The binary-TCs interaction is found to be sensitive to the relative orientation of the two TCs embedded in the MT. When the two cyclones are lined up in a northeast-southwest (NE-SW) orientation, the MT steers the two cyclones to approach each other and promotes the Fujiwhara effect. In contrast, when the initial cyclones are orientated in the northwest-southeast (NW-SE) direction of the MT, they will move away from each other under the large-scale steering flows.

Idealized simulations are conducted to understand how the MT and the β-effect influence the binary TC interactions, focusing on NE-SW oriented pairs. The steering flows at different stages are examined by partitioning them into the one from the MT and the other cyclone in the pair. The analysis shows that the binary TCs' motions are mainly controlled by the large-scale steering flows in the initial stage. In the case of binary TCs with a NE-SW orientation, the MT can promote two TCs to approach each other, thus increasing the possibility of binary interactions.

The sensitivity of the binary TCs interaction to their intensities, the strength of the MT, and the β-effect are examined. The stronger the MT, the stronger its large-scale steering flows will be, thus making the two NE-SW oriented TCs merge faster. Furthermore, the binary interaction is stronger on the β-plane compared to f-plane. It is likely due to the β-induced Rossby wave energy dispersion. As the MT evolves into a monsoon gyre (MG) -like pattern, a pronounced southwesterly flow emanates in the southeast quadrant of MG. This southwesterly flow acts as a steering flow to help the western TC (TCW) move northeastward, by which accelerates to reach the critical distance.

Keywords: Monsoon trough; Fujiwhara effect; Binary Tropical Cyclones

1. Introduction

The 'Fujiwhara effect' (also identified as the Fujiwhara interaction or a binary interaction) refers to the interaction of two or more cyclones, including mutual rotating, approaching, and merging (Fujiwhara 1921, 1923; Lander and Holland 1993). When two cyclonic vortices at a reasonably close distance experience a Fujiwhara interaction, they can be called the binary tropical cyclones (BTCs, Ren et al. 2020). Numerous modeling and observational studies have been conducted to investigate the interaction of BTCs. Dritschel and Waugh (1992) classified five most common Fujiwhara interactions using the idealized model: complete merger (CM), partial merger (PM), complete straining-out (CSO), partial straining-out (PSO), and elastic interaction (EI). Among them, the first two, CM and PM, are strong interactions. Based on the observations, Carr and Elsberry (1998) categorized the binary TCs interactions into direct TC interactions (DTIs), semidirect TC interactions (STIs), and indirect TC interactions (ITIs).

Some studies have focused on possible factors affecting the Fujiwhara interactions. Observational evidence by Brand (1970) suggested that two TCs interact when their initial separation distance is within 1400 km in the Western North Pacific (WNP). When the distance is less than 750 km, two TCs will attract to each other. Wang et al. (1989, 1992a, 1992b) found that the relative motion of the binary vortices is sensitive to their initial spacing and relative intensity. They also confirmed the existence of the critical separation distance (CSD) for the Fujiwhara interaction. The CSD is used to determine the BTCs (DeMaria and Chan 1984; Ritchie and Holland 1993; Wang and Holland

1995). Ren et al. (2020) used the CSD to establish an objective definition of binary TCs, and explore typical BTCs interaction. Within the CSD, BTCs have multiple manifestations, including merging. However, different CSDs were obtained in different model frameworks. For example, Ritchie and Holland (1993) found that, in a barotropic model, the initial separation distance between two TCs must be less than 300 km in order for them to merge. Also using a baroclinic model, Wang and Holland (1995) showed that the two vortices separated by less than 450 km are likely to merge. These previous studies focused on the binary interaction in the absence of environmental flows. In a real world, the behavior of multiple tropical cyclones is more complicated due to the wide range of scales involved in the environmental flow. Dong (1980) found that the anticlockwise mutual rotation of two TCs in the cyclonic environmental fields is largely influenced by the environmental flow through analyzing real cases. Hart and Evans (1999) also found that the cyclonic mutual rotation of two TCs accelerates when they are embedded in an environment with large-scale cyclonic vorticity. Kuo et al. (2004) identified the role of vorticity strength ratio and vorticity radius ratios between two TCs on the merger and formation of concentric vorticity.

Globally, the WNP basin has the highest frequency of TC formations, and thus multiple TCs often co-exist therein. In the summertime, the monsoon trough (MT) serves as the most prominent large-scale system in the WNP. It manifests itself as the near-equatorial confluence or the shear zone between the lower-level westerly monsoon and easterly trade winds (Briegel and Frank 1997; Holland 1995; Lander 1996; Chan and Evans 2002). The observations indicate that typhoons Noru and Kulap in 2017, which are oriented in NE-SW direction embedded in the MT, interacted and merged at the initial distance of 1800 km. However, two TCs Noul and Dolphin in 2015, which are located in the MT with a NW-SE orientation and distance of 1500 km, did not merge. The observational analysis presented in the next section will illustrate that there are distinct behaviors of two TCs within the MT. The two TCs in the MT can exhibit various types of Fujiwhara effects depending on the relative strength of two TCs, their characteristics in the MT, and the intensity of the MT. A better understanding of such occurrences could help to improve the perspective of TC track forecasts. This motivates us for this study. As our focus is to investigate strong Fujiwhara interactions, the CSD mentioned above refers to the threshold distance beyond which strong Fujiwhara interactions, such as PM and CM, occur.

This paper is organized as follows: Section 2 presents the characteristics of the two real cases in the observations, a pair of two typhoons Noru and Kulap in 2017 and Noul and Dolphin in 2015. Section 3 describes the model configuration of idealized simulations and experimental design. The simulated results for binary TCs in two different environmental characteristics and possible mechanisms involved are discussed in sections 4 and 5, respectively. A summary of the study is presented in section 6.

2. Analysis of two cases with binary TCs

Two distinctively different binary TCs behaviors within the MT region are presented. Scenarios of typhoons Noul and Dolphin in 2015, and Noru and Kulap in 2017 that are oriented in different directions embedded in the MT are selected to illustrate different impacts of the MT on the interactions between the two cyclones. The TC data are obtained from the best track dataset at the Japan Meteorological Agency (JMA). The global reanalysis representing the environmental flows is from the National Centers for Environmental Prediction (NCEP) global final analyses (FNL) data (NCEP 2000). The horizontal resolution of the reanalysis data is 1.0°×1.0° with a 6-hourly time interval.

Typhoon Noru and Kulap were embedded in the MG with a NE-SW orientation (Fig. 1c). Figures 1a and 1b present the 12-hourly track positions of the two storms and their relative positions. At 00 UTC 23 July, the separation distance is about 1800 km. From this point, Kulap moved westward while Noru moved southeastward. As the two TCs approached each other, they started rotating anticlockwise around each other (Fig. 1a and 1b). Kulap weakened as it approached Noru, and their mutual rotation speed started slowing. The two vortices partially merged on 28 July (Fig. 1d).

In contrast, Noul and Dolphin were located in the MT with a NW-SE orientation on May 4, 2015 (Fig. 2c). Note that since the track record of Dolphin from JMA started on 12 UTC 6 May, the track before that was based on the reanalysis data. The two typhoons' initial separation distance is about 1500 km (Fig. 2c). Dolphin moved southeastward under the westerly flows from the south side of the MT and then turned northward on 8 May (Fig. 2a). Noul basically maintained its northwestward movement under the easterly flows from the northern flank of the MT. The distance between the two TCs keeps getting larger and there is no rotation between them (Fig. 2b, 2d).

It has been well realized that TC motion is influenced by large-scale environmental steering flows, the β-drift, and possibly the circulation of a neighboring TC. A Tukey window spatial low-pass filtering will be used to separate the environmental flow from the TC-scale circulation (Hendricks et al. 2011; Ge et al. 2013, 2018; Xu et al. 2016; Dong and Neumann 1983). Systems with a wavelength greater than 1000 km are treated as the environmental fields, and those with a wavelength less than 1000 km are considered as the TC-scale system for the storm. It is worthwhile mentioning that different separating wavelengths have been tested, and the results are similar for the separation wavelength ranging from 500 to 1000 km.

After the separation of spatial scales, the steering flows from the MT and TCs are obtained by averaging the wind over an area within a radius of 400 km centered at the storm. For different intensities of TCs, different vertical layers have been used for a vertical average to better represent the steering flows instead of using a single-level field (Wu et al. 2011; Dong and Neumann 1983). Among the two selected real cases, Noul and Noru were the stronger ones within their own pairs. In the Noul-Dolphin pair, Noul’s central minimum sea-level pressure (CMSLP) decreased from 1006 hPa to 935 hPa during the period of interest, while Noru in the Noru-Kulap pair decreased from 985 hPa to 970 hPa and then weakened to 975 hPa. Typhoon Dolphin and Kulap were weaker in their respective pairs, with Dolphin’s intensity strengthening from 1007 hPa to 998 hPa during the period, while Kulap’s intensity remained roughly unchanged at around 1002 hPa. Following Wu et al. (2011), the vertical averages between 925–250 hPa are selected as the steering layer for Noul and Noru, and the averages between 850–500 hPa are used as the steering layer for Dolphin and Kulap.

With mainly westerly and easterly flows on the south and north side of the MT, Noru and Kulap with a NE-SW orientation initially have their separation distance decreasing with time (Fig. 1b). After 00 UTC 23 July, the MT evolves into a MG. The time evolutions of the steering flows at different scales for Noru and Kulap are displayed in Figs. 3a and 3b, respectively. After 00 UTC 25 July, the dual-vortex interaction gradually strengthened (Fig. 1b). Specifically, the zonal component (C_x) of Noru's movement conformed well with the large-scale steering flows before 18 UTC 25 July (Fig. 3a). Hereafter, Noru's C_x turned from positive to negative, and the deviation of it from C_{xL} increased. The difference between C_x and C_{xL} for Kulap, the weak cyclone of the pair, was large throughout. The meridional movement speed (C_y) for both Noru and Kulap is different from the large-scale steering flow (C_{yL}), especially after 12 UTC on 24 July, with Noru deviating to the north and Kulap to the south, and the difference reaches about 2–3 $\mathrm{m\ s^{-1}}$. The difference between C_x and C_{xL} of Kulap remains about 2 $\mathrm{m\ s^{-1}}$ after 00 UTC 27 July, when Kulap moves westward and merges with the eastward-moving Noru. Overall, the MT steering cannot fully explain the storms' movement for this case. The underlying processes that account for the discrepancy of movement speed may come from the strong mutual interactions between the two TCs and the idealized simulations will investigate it.

For the case of Noul and Dolphin, which had a NW-SE orientation, the moving speed of the weaker Dolphin in general conformed with the environmental MT flow (Fig. 4). Noul maintained a westward movement, and Dolphin kept eastward under the mainly zonal large-scale steering flow. The C_{yL} of Noul and Dolphin remained nearly 0 $\mathrm{m\ s^{-1}}$ from 00 UTC 4 May to 18 UTC 7 May. The largest difference between the TC movement and the environmental MT steering is with the zonal component of Noul for about 1–2 $\mathrm{m\,s^{-1}}$. The rather unique locations of the two storms allow the MT to push the two systems away from each other with no interactions between them.

The above results suggest that for a nearly east-west trough, when the two TCs are embedded in the MT at a certain orientation, their future motions can be very different as influenced by the MT steering forces. Ideal numerical experiments will be conducted to understand the influence of MT on the binary TCs interaction with different orientations.

3. Model and experimental designs

In this study, the Advanced Research version of the Weather Research and Forecasting model (WRF-ARW) is used for the idealized numerical experiments. The simulations use a single domain without nesting with a horizontal resolution of 18 km, and 55 levels in the vertical. The domain covers 6 °S – 33 °N, 118.5 °E – 179.5 °W. The periodic boundary conditions are applied in the east-west direction, and open boundary conditions are applied in the north-south boundary. The selected physics parameterizations are the WRF Single-Moment 6-class (WSM6; Hong et al. 2010) microphysics scheme, the Dudhia (1989) shortwave radiation scheme, the Rapid Radiative Transfer Model (RRTM; Mlawer et al. 1997) longwave radiation scheme, the Yonsei University planetary boundary layer (PBL) scheme (Hong et al. 2006) and the Kain-Fritsch cumulus parameterization scheme (Kain and Fritsch 1992). In this study, for those β-plane runs, the β value is set to 2.21×10^{-11} $\mathrm{m^{-1}\,s^{-1}}$, which corresponds to the center latitude (i.e., 15°N).

Based on the analysis presented in Section 2, eleven sets of numerical experiments are designed to reveal possible roles of the MT and the initial characteristics of the two TCs on the TC interactions (Table 1). The MT over the WNP features low-latitude cyclonic shear vorticity. In this study, the MT is defined as the shear zone between an easterly and a westerly between 5°–25°N centered at around 15°N (Guinn and Schubert 1993; Ferreira and Schubert 1997). The MT has a baroclinic structure with a transition at 400 hPa to an anticyclonic shear above. The horizontal distribution and vertical structure of the idealized MT are given in Fig. 5. The zonal wind profile of the initial MT is established as:

$$U(y) = -U_{m0} \cdot [\frac{y-y_0}{y_m} \cdot e^{0.5\cdot[1-(\frac{y-y_0}{y_m})^2]} \cdot \sin(\frac{\pi}{2} \cdot \frac{\sigma-0.4}{1-0.4})] \tag{1}$$

where $U(y)$ represents the zonal wind, U_{m0} is the maximum zonal wind, y is the meridional distances, y_0 represents the initial MT center, y_m indicates the half-width, which is taken as 900 km; σ is the model sigma level.

The initial TC wind speed is maximum at low level, decreases gradually with height, and vanishes at 100 hPa. That is, the tangential wind profile of initial TC is given by Equation (2):

$$V_t = \begin{cases} V_{\max} \cdot \left[\frac{r^2}{r_m^2} \cdot e^{1-\frac{r}{r_m}} \cdot \sin\left(\frac{\pi}{2} \cdot \frac{\sigma-0.1}{1-0.1} \right) \right] & , \ r \le r_m \\ V_{\max} \cdot \left[\frac{r}{r_m} \cdot e^{1-\frac{r}{r_m}} - \frac{|r-r_m|}{r_0-r_m} \cdot e^{1-\frac{r_0}{r_m}} \right] \cdot \sin\left(\frac{\pi}{2} \cdot \frac{\sigma-0.1}{1-0.1} \right) & , \ r > r_m \end{cases} \tag{2}$$

where V_t is tangential wind, r is the radius, V_{max} is maximum tangential wind, r_m is the radius of V_{max}, and r_0 represents the radius of tangential wind vanished. For TC, r_m and r_0 are 100 km, 1500 km respectively in idealized experiments.

Since the interaction between the two NE-SW oriented TCs in the MT presents a more interesting scenario, as shown by the example in Fig. 1, it is this study's main focus. In the control experiment "NE-CTL", two idealized TC-like vortices are embedded in the zonally oriented MT with a NE-SW orientation at the initial time. The two vortices are specified with different initial intensities. The strong one has a maximum wind speed (V_{max}) of 30 m s^{-1} and the weak storm of 10 m s^{-1}, both at a radius of 100 km. Given the specified two vortices, the CSD is 1111.3 km according to the Liou-Liu empirical formula (Liou et al. 2016). The initial distance between the two vortices is therefore set to 1200 km, which is unfavorable to their interactions. To investigate the role of the MT on Fujiwhara interaction, the monsoon trough is excluded in the experiment "NE-NMT". In the third experiment "NE-WMT", the strength of the MT is reduced by 20%. To further explore the effect of the relative strength of the initial vortices on the BTCs interaction, experiments "NE-SVI" and "NE-LVI" are set up with the same separation distance of the two TCs as in the NE-CTL but with different relative intensities (Table 1). Here "SVI" (LVI) is the abbreviation for the same (low) vortex intensity ratio. It should be noted that the relative intensity is defined as the ratio of the initial maximum wind speed of the western vortex to the eastern one.

In experiments "NW-CTL", "NW-SVI", and "NW-LVI", the two TC vortices are initially positioned in a NW-SE orientation embedded in the MT, representing the characteristics of the Noul-Dolphin couplets (Fig. 2). The three experiments carry the same intensities for the two TCs as in NE-CTL, NE-SVI, and NE-LVI. For brevity, the vortex initially located on the west side is identified as TCW, and the one on the east side is TCE in this study. In addition, a set of f-plane experiments are conducted for different relative intensities and relative positions of two TCs to investigate the β-effect on binary interactions. Three additional sets of NW-SE experiments are conducted, in which the idealized MT is centered around 7°N that is closer to the Noul-Dolphin case (Fig. 2). These experiments have similar results to those in which the MT's center is placed at 15°N (Figure not shown).

4 Binary TCs with northeast-southwest orientation

4.1 The role of the monsoon trough

a). Simulated Results

Figures 6–7 display the tracks, relative positions, and the evolution characteristics of the two TCs in NE-CTL, NE-NMT, and NE-WMT. In NE-CTL, the two vortices are initially located on either side of the MT within a NE-SW orientation. Due to the steering of the MT circulation, TCW in the NE-CTL moves northeastward and TCE moves northwestward so that the two TCs slowly approach each other and the cyclone-cyclone interaction strengthens. Subsequently, the two vortices rotate anticlockwise around each other (Fig. 6d). It is worth mentioning that after t = 48 h, the idealized zonal MT flow gradually evolves into a large cyclonic flow (Fig. 7d). By t = 72 h, TCE has moved to north of TCW. Meanwhile, the distance between TCW and TCE gradually decreases, and the distortion of the vortices increases (Fig. 7g). These two storms begin to merge at around t = 120 h (Fig. 7j). The MT is now a large MG, very similar to the MG in the Noru-Kulap case (Fig. 1c). In this study, when the large-scale environmental flow evolves into a sub-circular cyclonic vortex with a radius above 800 km, the MT is considered to evolve into an MG (Lander 1994; Wu et al. 2013; Molinari and Vollaro 2017). It should be noted that, under the idealized framework, the structure of the idealized MT is difficult to maintain in the absence of environmental weather systems (e.g., subtropical high). Dynamically, the MT region satisfies the necessary condition of barotropic instability, which leads to wave breakdown and evolves into several vortices (Guinn and Schubert 1993).

In contrast, the behaviors of TCW and TCE show marked differences in NE-NMT. Since there is no large-scale steering flow, the vortex pair only exhibit their individual northwestward movement under the β-drift effect (Fig. 6b). There is little change of the distance between TCW and TCE. Meanwhile, by testing the binary interaction in absence of MT with different initial spacings from 400–800 km, it is found that TCW and TCE will merge when they are separated by approximately less than 500 km initially. The weaker TCE deforms and merges into the spiral rainband of stronger TCW under the strong Fujiwhara effect (Figure not shown). The above results show that MT can advect the two TCs and make them close enough to occur the Fujiwhara interactions.

In NE-WMT with reduced MT intensity, the evolution characteristics of TCW and TCE are similar to those of NE-CTL. However, there remains a significant distance between the two vortices at the end of the integration t = 120 h, as the approaching speed of the two cyclones is slower with weaker steering by the MT and the two entities miss the window of opportunity to merge together (Fig. 6f). As mentioned above, the circulation of MT is likely to facilitate the two TCs' merging, as well as the merging rate, which is sensitive to the MT strength. The merging rate is represented by the relative distance between two TCs during the integration period of 120 h. The results suggest that the MT can significantly affect the Fujiwhara effect of two TCs, in agreement with previous studies (Brand 1970; Wang and Holland 1995; Wang et al. 1989).

b). Decomposition of steering flows at different scales

As with the real cases discussed in Section 2, the MT and typhoon-scale flows can be separated using the spatial filtering method (Ge et al. 2013; Xu et al. 2016). Since the TC-scale circulation contains both TCW and TCE, we also separate out the circulation associated with each individual TC. We attempt to obtain the system-scale circulation by partitioning and reconstructing the wind field in a limited vortex core area (Zhou and Cao 2010; Cao et al. 2019). Specifically, we first extract one TC from the total fields (i.e., the TCE) with its circulation confined within a region with “0” contour in the relative vorticity. The stream function and velocity potential are then calculated based on the finite region’s vorticity and divergence. Then the associated rotational and divergent winds are obtained. Finally, the storm-scale circulation is obtained by adding the rotational and divergent flows together. By subtracting the circulation of TCE from the filtered system-scale circulation, the remaining total TC circulation is taken as the circulation of TCW. The same method can be applied to extract the TCW.

Separating the large-scale monsoonal flow from the storm-scale circulation of each TC can better reflect the relative significance of the BTCs interaction and the large-scale steering flow on the TC’s movement. In our idealized numerical experiments, the averaged value of different steering flows from different vertical layers is selected depending on the strength of the vortex (Wu et al. 2011; Dong and Neumann 1983). The vertical average between 1–10 km is selected as the steering layer for the stronger TC, and the average of 1–6 km is obtained as the steering layer for the weaker one, respectively. At each level, the steering flows from the different scales are obtained by averaging the wind fields within a radius of 500 km centered at the storm.

Figure 8 presents the time series of different components of the steering flows in NE-CTL associated with MT, TCW, and TCE separately. In the early stage (i.e., t = 0–48 h), for both TCW and TCE, their movements are primarily controlled by the MT steering, since the movement speeds closely match with the components derived from the MT flow. During the next 24 hours (t = 48–72 h), the TCW is still steered by the monsoonal flow, but TCE exhibits different evolution features. For instance, the contribution from TCW for TCE starts to become significant shortly after 48 h. However, the impact of TCE on TCW is not evident until t = 72 h, while the distance between TCE and TCW consistently decreases since the start (Fig. 6a, d).

To summarize, TCW first moves northeastward under the large-scale steering flow and then experiences a re-curvature to be northwestward around t = 108 h under the combined effect of the TCE and the MT. For TCE, it is affected by the MT before 48 h, and then experiences an anticlockwise movement with combined effects from the MT and TCW. The reason that the TCE is affected by TCW earlier is due to the size differences between them so that the weaker cyclone is attracted by the stronger one quicker. The steering flows in the meridional and zonal directions display similar characteristics, except that the meridional component of TCE is completely controlled by the TCW beyond 72 h (Fig. 8d) during the looping of TCE by the TCW (Fig. 6a). The overall process is similar to the merging of Noru and Kulap (Fig. 1).

In NE-NMT, TCW and TCE do not approach each other, and both two entities show steadily northwestward movements due to the β-effect (Fig. 6b, e). The study of Chan and Williams (1987) suggests that the β-drift is largely proportional to the TC size. As a stronger TC tends to have a larger outer size, it has a larger northwestward propagation speed than TCE. Therefore, the β-effect can drive clockwise rotation of two TCs relative to their midpoint. In NE-WMT (Fig. 9), the weakening of MT inevitably leads to a correspondingly smaller large-scale steering flow, slowing down the TCW and TCE's approach to each other. As a result, the time when TCW and TCE starts interacting lags behind that in NE-CTL but the overall patterns are similar between NE-CTL and NE-WMT. In NE-WMT, the contribution from TCW to TCE beyond 72h (Fig. 9d) is much less than its counterpart in NE-CTL (Fig. 8d), indicating a later merger between the two cyclones.

4.2 Sensitivity of relative intensity and the β-effect

The binary vortices in the first three experiments all have a NE-SW orientation and the same relative intensities of the binary TCs. Because the relative intensity of the two TCs can have a wide range in real cases, two more experiments are conducted to investigate the sensitivity of TC interactions to their relative strength. In NE-SVI, the intensities for the two TCs are the same of 30 m s^{-1} maximum wind, while in NE-LVI, the TCW and TCE have 10 m s^{-1} and 30 m s^{-1}, respectively. In both experiments, the initial positions of the two TCs are the same as in NE-CTL.

Figure 10 presents the tracks and the relative positions of the binary TCs' center in NE-SVI and NE-LVI experiments. For better comparison, Fig. 6a and 6d for NE-CTL are also included in Fig. 10. In general, regardless of their relative intensities, the binary TCs rotate anticlockwise and approach each other under the large-scale steering flows and experience the Fujiwhara effect, and all eventually merge. In NE-SVI, the two equally strong TCs approach to each other faster than in NE-CTL and experience two looping motions (Fig. 10b, e). Meanwhile, the TCW's intensity weakens gradually, thus favoring their faster merge than in NE-CTL (Figure not shown). In NE-LVI, the stronger TCE moves northwestward during t = 0–24 h. Then, after a short southward motion during t = 24–42 h, it moves northwestward steadily under the MG circulation and a strong β-effect, while the weaker TCW moves mostly eastward in the early stage under the influence of the MG with a weaker β-effect and then it moves northward under the influence of TCE. The two cyclones loop around each other in the early stage and merge after 87h (Fig. 10f). Although the β-drift of TCE favors it to move northwestward, the weaker TCW's intensity weakens quickly, which is conducive to the stronger TCE to approach to TCW.

The evolution of different components of the steering flows at different scales for NE-SVI and NE-LVI are given in Fig. 11. As the two cyclones get closer, it is difficult to separate the steering components from one another, only the periods before the two vortices got closer than 370 km are shown for NE-SVI and NE-LVI. In NE-SVI, the Fujiwhara interaction starts to appear after 39 h. Because both TCW and TCE are strong typhoons in this case, both of them undergo multiple turns before eventually merging. Beyond 60h, the binary TCs interaction is significant, as shown by the large contribution of the steering of one TC to the other, reflecting the interactions of the two vortices. In NE-LVI, the weaker typhoon TCW approaches TCE rapidly after 24 h as a result of the combined effect of the large-scale steering flows and different intensities of the two cyclones. Meanwhile, the stronger TCE is basically controlled by the large-scale steering flows, and the influence of TCW on it is small (Fig. 11d, h). These idealized simulations reflect many characteristics of the evolution of the Noru and Kulap, indicating that when the binary TCs are initially oriented NE-SW in the MT, the large-scale steering flows are conducive to the merger of two TCs.

In comparison with the evolutions of the binary vortices in NE-CTL, NE-SVI, and NE-LVI, the dual storms only partially merge in the NE-CTL, while a complete merging has occurred in NE-SVI and NE-LVI. According to the NE-NMT experiment, a clockwise (anticlockwise) mutual rotation of the two TCs occurs in NE-CTL (NE-LVI), relative to the midpoint of the two TCs. It is speculated that this clockwise rotation is ascribed to the different β-drift associated with the storm size. In NE-NMT, TCW has a larger outer size and thus has a larger β-drift. As such, it has a larger northwestward propagation speed compared to its counterpart (TCE), which likely induces the clockwise mutual rotation. Likewise, the difference in β-drift can account for a clockwise (anticlockwise) mutual rotation in NE-CTL (NE-LVI), relative to the midpoint of the two TCs.

To explore more specifically the role of the β-effect, the three NE-SW oriented experiments with the same relative intensities as in NE-CTL, NE-SVI, and NE-LVI are conducted on the f-plane, identified with "F" in front of the experiment names (Table 1), and their tracks and relative positions are given in Fig. 12. In FNE-CTL and FNE-LVI, the relative distances between two TCs are both approximately 300 km around t = 120 h. Of particular interest is that the weaker TC approaches and rotates around the strong one. Thereafter, the weak TC becomes the outer spiral rain band of the strong TC (Figure not shown). In the absence of the β-effect, the two vortices in FNE-CTL and FNE-LVI have nearly mirroring trajectories, and their approaching speed is similar. In FNE-SVI, the lack of β-effect makes the TCs rotate with each other in a symmetric way with their equal intensities under the influence of MT. In summary, two TCs with large size differences are more likely to interact than those with identical sizes.

Furthermore, the results above indicate that the binary interaction is faster on the β-plane compared to f-plane. As the β-effect likely affects large-scale environmental flow, the evolutions of the large-scale circulation in NE-LVI and FNE-LVI are shown in Fig. 13. Previous studies (Carr and Elsberry 1995; Bi et al. 2015) have pointed out that Rossby wave energy dispersion contributes to a sudden northward track change of TC. As MT evolves into MG, a pronounced southwesterly flow emanates due to the β-induced energy dispersion (Ge et al. 2008). An anticyclone, therefore, develops in the southeastern flank of MG. This pattern enhances the pressure gradient and thus the southwesterly flow therein. This flow acts as a steering flow to help TCW move northeastward, which accelerates to reach the CSD (top panels in Fig. 13). With this regard, the β-effect can impact the approaching speed of two TCs and thus Fujiwhara effect, which is in agreement with Chan and Law (1995).

5 Binary TCs with northwest-southeast orientation

In the two observational cases, both the tropical cyclone couplets Noru-Kulap and Noul-Dolphin, are located in the MT, but showed completely different tracks. This indicates that the relative position of the two storms embedded in the MT may affect their interactions (Fig.1-2).

Figure 14 displays the tracks, and relative positions of the two TCs in NW-CTL, NW-SVI, and NW-LVI. All the systems are embedded in the NW-SE direction in the MG, and have the same storm intensities as their counterparts in NE-CTL, NE-SVI and NE-LVI, respectively. In NW-CTL, the two TCs initially drift away from each other without a mutual rotation. Their initial relative motions are similar to the movements of Noul-Dolphin. Nevertheless, after t = 60 h, the two vortices have some rotation around each other. In NW-SVI, the two TCs exhibit a more distinct mutual rotation during t = 0–69 h (Fig. 14e). Furthermore, the two vortices in NW-LVI rotate with each other during the integration period (Fig. 14f).

To further demonstrate these discrepancies, the evolutions characteristics of the two TCs in NW-CTL, NW-SVI, and NW-LVI are given in Fig. 15. In NW-CTL, as the TCW is stronger, a cyclonic vortex with a radius over 800 km forms near the strong TC. MT still evolves into MG through the interaction with the TCs. The southwesterly winds are strengthened on its southeast side due to the energy dispersion. This contributes to the separation of TCW and TCE (left panels in Fig. 15). In NW-SVI, since both TCW and TCE are intense TCs, the southwesterly winds on the southeast side of TCE are enhanced more significantly. The enhanced southwesterly flow likely helps TCW move faster to turn northeastward, thus making the TCW and TCE exhibit mutual rotation (middle panels in Fig. 15). Similarly, as the MT evolves into MG through the interaction with the TCs, the TCW moves to the southwest after several track swings under the effect of MG in NW-LVI (right panels in Fig. 15). Once again, due to the lack of the constrain of larger circulation (e.g., subtropical high), the structure of MT cannot be maintained.

The evolution of each steering flow component from different scales for NW-CTL, NW-SVI, and NW-LVI are given in Figures 16-17. In these experiments, the initial two TCs depart from each other under the influence of easterly and westerly flows on either side of the MT. During the 120 h of integration, the actual speeds of TCW and TCE are in good agreement with the large-scale steering flows regardless of their relative intensities. Meanwhile, the impact of adjacent TC fluctuates around zero during the integration time in these NW-SE experiments. This indicates that the large-scale steering flows dominate the movements of TCW and TCE.

Overall, when the two vortices are located with a NW-SE orientation in the zonal MT, the easterly and westerly large-scale steering flows keep them away from each other, unfavorable for their merging. These findings are consistent with the similar theoretical model of Dong and Neumann (1983). Meanwhile, when the eastern TC is stronger, the β-effect favors more north and northwestward motion and pushes it away from the MT's westerly flow. As MT still evolves into MG through the interaction with the TCs, the southwesterly winds are strengthened on its southeast side due to the energy dispersion, thus making the TCW and TCE exhibit mutual rotation.

6 Discussion and summary

The observational analysis shows that a Fujiwhara effect occurs between two typhoons Noru and Kulap (2015), which are originally located on the two sides of the MT with a NE-SW orientation, and eventually merge. Conversely, Noul and Dolphin (2017) located in the MT with a NW-SE orientation move away from each other. It is worth noting that Noru-Kulap merges eventually with an initial distance of 1800 km apart. In contrast, Noul-Dolphin, separated initially by 1500 km, did not merge. The goal of this study is to examine the influence of MT on the interactions of two TCs by utilizing ideal numerical simulations.

The steering from the MT and from the other co-existing cyclone are separated out and analyzed. A conceptual model of how MT affects the BTCs interactions in different configurations is given in Fig. 18. When the two vortices are distributed in a NE-SW direction in the beginning, the MT flow plays an essential role for both cyclones at the early stage. The MT's circulation pushes the two cyclones closer and promotes the cyclone-cyclone interaction. Once two vortices approach within a short distance, the impact from the nearby TC becomes more evident, and the two TCs exhibit Fujiwhara interaction (Fig. 18a). In this set up, even if the two vortices are initially far apart, they can still interact with the help of the steering from the MT. Therefore, MT can accelerate the two TCs to move closer, thus the Fujiwhara interaction.

In addition, the dual-vortex interaction is sensitive to the MT's strength, the relative intensity of the two TCs, and the β-effect. The stronger the MT, the faster the two vortices approach each other and merge. Moreover, the binary interaction on the β-plane series is stronger than those on the f-plane. Once the MT evolves into an MG-like pattern, a pronounced southwesterly flow emanates due to the energy dispersion. This southwesterly flow acts as a steering flow to help TCW move northeastward, which accelerates to reach the CSD.

When the two TCs are located with a NW-SE orientation in the MT, the MT circulation pushes the two cyclones away from each other and further prevents the interactions between them (Fig. 18b). Therefore, the motion of two vortices will be controlled by the large-scale steering flows throughout. In such a configuration, the greater the relative intensity of the two storms, the faster they separate from each other.

In this study, the simulations are idealized. In reality, the MT structure is more complicated also. This implies that the binary TCs' development may highly depend on the morphology of the MT and TC structure. These issues need to be further addressed in future studies.

Acknowledgments. This work was jointly sponsored by the National Natural Science Foundation of China (42175003; 42088101). The numerical calculations in this paper have been done in the Supercomputing Center of Nanjing University of Information Science & Technology.

Data availability statement. The datasets generated and/or analyzed in this study are available from the corresponding author on reasonable request.

References

Bi, M., T. Li, M. Peng, and X. Shen, 2015: Interactions between Typhoon Megi (2010) and a Low-Frequency Monsoon Gyre*. *J. Atmos. Sci.*, **72**, 2682-2702.

Brand, S., 1970: Interaction of binary tropical cyclones of the western North Pacific Ocean. *J. Appl. Meteor.*, **9**, 433-441.

Briegel, L. M., and W. M. Frank, 1997: Large-scale influences on tropical cyclogenesis in the Western North Pacific. *Mon. Wea. Rev.*, **125**, 1397-1413.

Cao, Z., Q. Xu, and D.-L. Zhang, 2019: A new method to diagnose cyclone–cyclone interaction and its influences on precipitation. *J. Appl. Meteor. Climatol.*, **58**, 1821-1851.

Carr, L. E., and R. L. Elsberry, 1995: Monsoonal Interactions Leading to Sudden Tropical Cyclone Track Changes. *Mon. Wea. Rev.*, **123**, 265-290.

Carr, L. E., III, and R. L. Elsberry, 1998: Objective diagnosis of binary tropical cyclone interactions for the Western North Pacific Basin. *Mon. Wea. Rev.*, **126**, 1734-1740.

Chan, S. C., and J. L. Evans, 2002: Comparison of the structure of the ITCZ in the West Pacific during the boreal summers of 1989–93 using AMIP simulations and ECMWF reanalysis. *J. Climate*, **15**, 3549-3568.

Chan, J. C. L., and A. C. K. Law, 1995: The interaction of binary vortices in a barotropic model. *Meteorl. Atmos. Phys.*, **56**, 135–155.

Chan, J. C. L., and R. T. Williams, 1987: Analytical and Numerical Studies of the Beta-Effect in Tropical Cyclone Motion. Part I: Zero Mean Flow. *J. Atmos. Sci.*, **44**, 1257–1265.

Chen, L., and Z. Meng, 2001: An overview on tropical cyclone research progress in China during the past ten years. *Chin. J. Atmos. Sci.*,**25**, 420-432.

Chen, X., Y. Wang, and K. Zhao, 2015: Synoptic flow patterns and large-scale characteristics associated with rapidly intensifying tropical cyclones in the South China Sea. *Mon. Wea. Rev.*, **143**, 64-87.

DeMaria, M., and J. C. L. Chan, 1984: Comments on "A numerical study of the interactions between two tropical cyclones". *Mon. Wea. Rev.*, **112**, 1643-1645.

Dong, K., 1980: On the clockwise co-rotation of typhoon twins. *Meteor. Mon.*, **6**, 18-19.

Dong, K., and C. J. Neumann, 1983: On the relative motion of binary tropical cyclones. *Mon. Wea. Rev.*, **111**, 945-953.

Dritschel, D. G., and D. W. Waugh, 1992: Quantification of the inelastic interaction of unequal vortices in two‐dimensional vortex dynamics. *Phys. Fluids A*, **4**, 1737-1744.

Dudhia, J., 1989: Numerical study of convection observed during the winter monsoon experiment using a mesoscale two-dimensional model. *J. Atmos. Sci.*, **46**, 3077-3107.

Ferreira, R. N., and W. H. Schubert, 1997: Barotropic aspects of ITCZ breakdown. *J. Atmos. Sci.*, **54**, 261-285.

Fiorino, M., and R. L. Elsberry, 1989: Contributions to tropical cyclone motion by small, medium and large scales in the initial vortex. *Mon. Wea. Rev.*, **117**, 721-727.

Fujiwhara, S., 1921: The natural tendency towards symmetry of motion and its application as a principle in meteorology. *Quart. J. Roy. Meteor. Soc.*, **47**, 287-292.

Fujiwhara, S., 1923: On the growth and decay of vortical systems. *Quart. J. Roy. Meteor. Soc.*, **49**, 75-104.

Ge, X., T. Li, Y. Wang, and M. S. Peng, 2008: Tropical Cyclone Energy Dispersion in a Three-Dimensional Primitive Equation Model: Upper-Tropospheric Influence. *J. Atmos. Sci.*, **65**, 2272–2289.

Ge, X., T. Li, and M. Peng, 2013: Effects of vertical shears and midlevel dry air on tropical cyclone developments. *J. Atmos. Sci.*, **70**, 3859-3875.

Ge, X., Z. Yan, M. Peng, M. Bi, and T. Li, 2018: Sensitivity of Tropical Cyclone Track to the Vertical Structure of a Nearby Monsoon Gyre. *J. Atmos. Sci.*, **75**, 2017–2028.

Guinn, T. A., and W. H. Schubert, 1993: Hurricane spiral bands. *J. Atmos. Sci.*, **50**, 3380-3403.

Hart, R. E., and J. L. Evans, 1999: Simulations of dual-vortex interaction within environmental shear. *J. Atmos. Sci.*, **56**, 3605-3621.

Hendricks, E. A., M. S. Peng, X. Ge, and T. Li, 2011: Performance of a Dynamic Initialization Scheme in the Coupled Ocean–Atmosphere Mesoscale Prediction System for Tropical Cyclones (COAMPS-TC). *Wea. Forecasting*, **26**, 650–663

Holland, G. J., 1995: Scale interaction in the Western Pacific Monsoon. *Meteor. Atmos. Phys.*, **56**, 57-79.

Hong, S.-Y., K.-S. S. Lim, Y.-H. Lee, J.-C. Ha, H.-W. Kim, S.-J. Ham, and J. Dudhia, 2010: Evaluation of the WRF double-moment 6-class microphysics scheme for precipitating convection. *Adv. Meteor.*, **2010**, 185-194.

Hong, S. Y., Y. Noh, and J. Dudhia, 2005: A new vertical diffusion package with an explicit treatment of entrainment processes. *Mon. Wea. Rev.*, **134**, 2318.

Kain, J. S., and J. M. Fritsch, 1992: The role of the convective "trigger function" in numerical forecasts of mesoscale convective systems. *Meteor. Atmos. Phys.*, **49**, 93-106.

Kuo, H. C., L. Y. Lin, C. P. Chang, and R. T. Williams, 2004: The formation of concentric vorticity structures in typhoons. *J. Atmos. Sci.*, **61**, 2722-2734.

Lander, M. A., 1994: Description of a Monsoon Gyre and Its Effects on the Tropical Cyclones in the Western North Pacific during August 1991. *Wea. Forecasting*, **9**, 640–654.

Lander, M., and G. J. Holland, 1993: On the interaction of tropical-cyclone-scale vortices. I: Observations. *Quart. J. Roy. Meteor. Soc.*, **119**, 1347-1361.

Lander, M. A., 1996: Specific tropical cyclone track types and unusual tropical cyclone motions associated with a reverse-oriented monsoon trough in the Western North Pacific. *Wea. Forecasting*, **11**, 170-186.

Lau, K.-H., and N.-C. Lau, 1992: The energetics and propagation dynamics of tropical summertime synoptic-scale disturbances. *Mon. Wea. Rev.*, **120**, 2523-2539.

Li, L., and X. Ge, 2020: Intensity Change of NORU (2017) During Binary Tropical Cyclones Interaction. *Asia-Pac. J. Atmos. Sci.*, **57**, 1-13.

Liou, Y.-A., and R. S. Pandey, 2020: Interactions between typhoons Parma and Melor (2009) in North West Pacific Ocean. *Wea. Climate Extremes*, **29**, 100272.

Liou, Y.-A., J.-C. Liu, C.-C. Liu, C.-H. Chen, K.-A. Nguyen, and J. P. Terry, 2019: Consecutive Dual-Vortex Interactions between Quadruple Typhoons Noru, Kulap, Nesat and Haitang during the 2017 North Pacific Typhoon Season. *Remote Sens.*, **11**., 1843-. http://dx.doi.org/10.3390/rs11161843

Liou, Y.-A., J.-C. Liu, M.-X. Wu, Y.-J. Lee, C.-H. Cheng, C.-P. Kuei, and R.-M. Hong, 2016: Generalized empirical formulas of threshold distance to characterize cyclone–cyclone interactions. *IEEE Trans. Geosci. Remote Sens.*, **54**, 3502-3512.

Mlawer, E. J., S. J. Taubman, P. D. Brown, M. J. Iacono, and S. A. Clough, 1997: Radiative transfer for inhomogeneous atmospheres: RRTM, a validated correlated‐k model for the longwave. *J. Geophys. Res.: Atmos.*, **102**.

Molinari, J., and D. Vollaro, 2011: A subtropical cyclonic gyre associated with interactions of the MJO and the midlatitude jet. *Mon. Wea. Rev.*, **140**, 343-357.

Molinari, J., and D. Vollaro, 2017: Monsoon Gyres of the Northwest Pacific: Influences of ENSO, the MJO, and the Pacific–Japan Pattern. *J. Climate*, **30**, 1765–1777.

NCEP, 2000: NCEP FNL Operational Model Global Tropospheric Analyses, continuing from July 1999.

Okubo, A., 1970: Horizontal dispersion of floatable particles in the vicinity of velocity singularities such as convergences. *Deep-Sea Res. Oceanogr. Abstr.*, **17**, 445-454.

Ren, F., Y. Xie, B. Yin, M. Wang, and G. Li, 2020: Establishment of an Objective Standard for the Definition of Binary Tropical Cyclones in the Western North Pacific. *Adv. Atmos. Sci.*, **37**, 1211-1221.

Ritchie, E. A., and G. J. Holland, 1993: On the interaction of tropical-cyclone-scale vortices. II: Discrete vortex patches. *Quart. J. Roy. Meteor. Soc.*, **119**, 1363-1379.

Rozoff, C. M., W. H. Schubert, B. D. McNoldy, and J. P. Kossin, 2006: Rapid filamentation zones in intense tropical cyclones. *J. Atmos. Sci.*, **63**, 325-340.

Tsai, Y.-M., H.-C. Kuo, and W. H. Schubert, 2010: Filamentation time diagnosis of thinning troughs and cutoff lows. *Mon. Wea. Rev.*, **138**, 2327-2335.

Ventham, J. D., and B. Wang, 2007: Large-scale flow patterns and their influence on the intensification rates of Western North Pacific tropical storms. *Mon. Wea. Rev.*, **135**, 1110-1127.

Wang, Y., and Y. Zhu, 1989: Interactions of binary vortices in a nondivergent barotropic model. *J. Trop. Meteor.*, **5**, 105-115.

Wang, Y., and Y. Zhu, 1992a: Analysis and numerical study of the interactions of binary tropical cyclones Part Ⅰ: Analysis of Physical Mechanism. *Chin. J. Atmos. Sci.*, **16**, 573-582.

Wang, Y., and Y. Zhu, 1992b: Mechanism analysis and numerical study on the interactions of binary tropical cyclones Part Ⅱ: Numerical Simulation. *Chin. J. Atmos. Sci.*, **16**, 659-668.

Wang, Y., and G. J. Holland, 1995: On the interaction of tropical-cyclone-scale vortices. IV: Baroclinic vortices. *Quart. J. Roy. Meteor. Soc.*, **121**, 95-126.

Weiss, J., 1991: The dynamics of entropy transfer in two-dimensional hydrodynamics. *Phys. D*, **48**, 273-294.

Wu, L., Z. Wen, R. Huang, and R. Wu, 2012: Possible linkage between the monsoon trough variability and the tropical cyclone activity over the Western North Pacific. *Mon. Wea. Rev.*, **140**, 140-150.

Wu, X., J.-f. Fei, X.-g. Huang, X.-p. Cheng, and J.-q. Ren, 2011: Statistical classification and characteristics analysis of binary tropical cyclones over the western north Pacific Ocean. *J. Trop. Meteor.*, **27**, 455-464.

Wu, L., Z. Ni, J. Duan, and H. Zong, 2013: Sudden Tropical Cyclone Track Changes over the Western North Pacific: A Composite Study. *Mon. Wea. Rev.*, **141**, 2597–2610.

Xu, M., S. Zhou, and X. Ge, 2016: An idealized simulation study of the impact of monsoon gyre on tropical cyclogenesis. *Acta Meteor. Sin.*, **74**, 733-743.

Yang, C.-C., C.-C. Wu, K.-H. Chou, and C.-Y. Lee, 2008: Binary interaction between typhoons Fengshen (2002) and Fungwong (2002) based on the potential vorticity diagnosis. *Mon. Wea. Rev.*, **136**, 4593-4611.

Zhou, Y.-s., and J. Cao, 2010: Partitioning and reconstruction problem of the wind in a limited region. *Acta Phys. Sin.*, **59**, 2898-2906.

List of Tables

Table 1. Summary of the idealized experiments.

Experiment	Monsoon trough	The $\boldsymbol{V_{max}}$ of western vortex (m/s)	The $\boldsymbol{V_{max}}$ of eastern vortex (m/s)	Initial orientation of two TCs	$\boldsymbol{\beta}$/ $\boldsymbol{f}$-plane
NE-CTL	Existence	30	10	NE-SW	β
NE-WMT	Existence (reduced 20%)	30	10	NE-SW	β
NE-NMT	Not existence	30	10	NE-SW	β
NE-SVI	Existence	30	30	NE-SW	β
NE-LVI	Existence	10	30	NE-SW	β
FNE-CTL	Existence	30	10	NE-SW	f
FNE-SVI	Existence	30	30	NE-SW	f
FNE-LVI	Existence	10	30	NE-SW	f
NW-CTL	Existence	30	10	NW-SE	β
NW-SVI	Existence	30	30	NW-SE	β
NW-LVI	Existence	10	30	NW-SE	β

List of Figures

Fig. 1. (a) The JMA 12-hourly best tracks of Noru (blue) and Kulap (red) from 00 UTC 23 July to 00 UTC 28 July 2017. The typhoon symbols denote the beginning and ending or the typhoon positions from the JMA best track data. The dashed line represents the TC's best tracks before it transitions to an extratropical cyclone. The solid line represents the time period of interest in this study; (b) The evolution of relative positions of two TCs. The origin (0, 0) is the middle point between two vortices at each time; (c)-(d) The 850 hPa wind (vector; unit: $\mathrm{m\ s^{-1}}$) and vorticity (shading, unit: $1 \times 10^{-5}\ \mathrm{s^{-1}}$) on 00 UTC 23 July and 00 UTC 28 July 2017.

Fig. 2. (a) The 12-hourly track positions of Noul (blue line) and Dolphin (red line) from 00 UTC 4 May to 00 UTC 9 May 2015. The typhoon symbols denote the beginning and ending or the typhoon positions from the JMA best track data. The dashed line represents the TC's best tracks before it transitions to an extratropical cyclone. The solid line represents the time period of interest in this study; (b) The evolution of relative positions of two TCs in which the origin (0, 0) is the middle point between two vortices at each time; (c)-(d) The 850 hPa wind (vector; unit: $\mathrm{m\ s^{-1}}$) and vorticity (shading, unit: $1 \times 10^{-5}\ \mathrm{s^{-1}}$) on 00 UTC 4 May and 00 UTC 9 May 2015, respectively.

Fig. 3. Evolutions of the steering flows at different scales of the Noru (left panels) and Kulap (right panels). $\mathrm{C_X}$ and $\mathrm{C_Y}$ (black lines) represent the TC's actual movement speed. $\mathrm{C_{XL}}$ and $\mathrm{C_{YL}}$ (blue lines) show the large-scale steering flow. X and Y denote the zonal and meridional components, respectively.

Fig. 4. As in Fig.3, but for Typhoon Noul (left panels) and Dolphin (right panels).

Fig. 5. Initial configurations of (a) 850 hPa wind fields of ideal MT and (b) vertical structure of zonal winds.

Fig. 6. The tracks (top) and relative positions (bottom) of TCW (black lines) and TCE (red lines) in NE-CTL (left panels), NE-NMT (middle panels), and NE-WMT (right panels) from t = 0 h to 120 h.

Fig. 7. Time evolutions of 850 hPa wind (vector; unit: $\mathrm{m\ s^{-1}}$) and vorticity (shading; unit: $1 \times 10^{-5}\ \mathrm{s^{-1}}$) in NE-CTL (left panels), NE-NMT (middle panels), and NE-WMT (right panels), respectively.

Fig. 8. Evolutions of the steering flows at different scales of the TCW (left panels) and TCE (right panels) in NE-CTL. $\mathrm{C_X}$ and $\mathrm{C_Y}$ (black lines) represent the actual moving speed of TC. $\mathrm{C_{XL}}$ and $\mathrm{C_{YL}}$ (blue lines) show the large-scale steering flow. $\mathrm{C_{XW}}$, $\mathrm{C_{YW}}$, $\mathrm{C_{XE}}$ and $\mathrm{C_{YE}}$ (red lines) present the impact of TCW and TCE on the other storm. X and Y denote the zonal and meridional components, respectively.

Fig. 9. As in Fig.8, but for NE-WMT.

Fig. 10. The tracks (top) and relative positions (bottom) of TCW (black lines) and TCE (red lines) in NE-CTL (left), NE-SVI (middle) and NE-LVI (right) from t = 0 h to 120 h.

Fig. 11. As in Fig.8, but for NE-SVI (left two panels), and NE-LVI (right two panels).

Fig. 12. The tracks (top) and relative positions (bottom) of TCW (black lines) and TCE (red lines) in FNE-CTL (left panels), FNE-SVI (middle panels), and FNE-LVI (right panels) from t = 0 h to 120 h.

Fig. 13. The tracks (top) and relative positions (bottom) of TCW (black lines) and TCE (red lines) in NW-CTL (left panels), NW-SVI (middle panels), and NW-LVI (right panels) from t = 0 h to 120 h.

Fig. 14. Evolutions of 850 hPa monsoonal wind (vector; unit: $\mathrm{m\ s^{-1}}$) and vorticity (shading; unit: $1 \times 10^{-6}\ \mathrm{s^{-1}}$) in NE-LVI (top panels) and FNE-LVI (bottom panels). The white “W” and “E” indicate the positions of TCW and TCE correspondingly at that moment. Vectors in red represent wind speeds greater than 10 $\mathrm{m\ s^{-1}}$.

Fig. 15. Time evolutions of 850 hPa wind (vector; unit: $\mathrm{m\ s^{-1}}$) and vorticity (shading; unit: $1 \times 10^{-5}\ \mathrm{s^{-1}}$) in NW-CTL (left panels), NW-SVI (middle panels), and NW-LVI (right panels), respectively.

Fig. 16. As in Fig.8, but for NW-CTL.

Fig. 17. As in Fig.8, but for NW-SVI (left two panels) and NW-LVI (right two panels).

Fig. 18. Conceptual model of the influences of monsoon trough on the BTCs interactions in the (a) NE-SW and (b) NW-SE configuration.

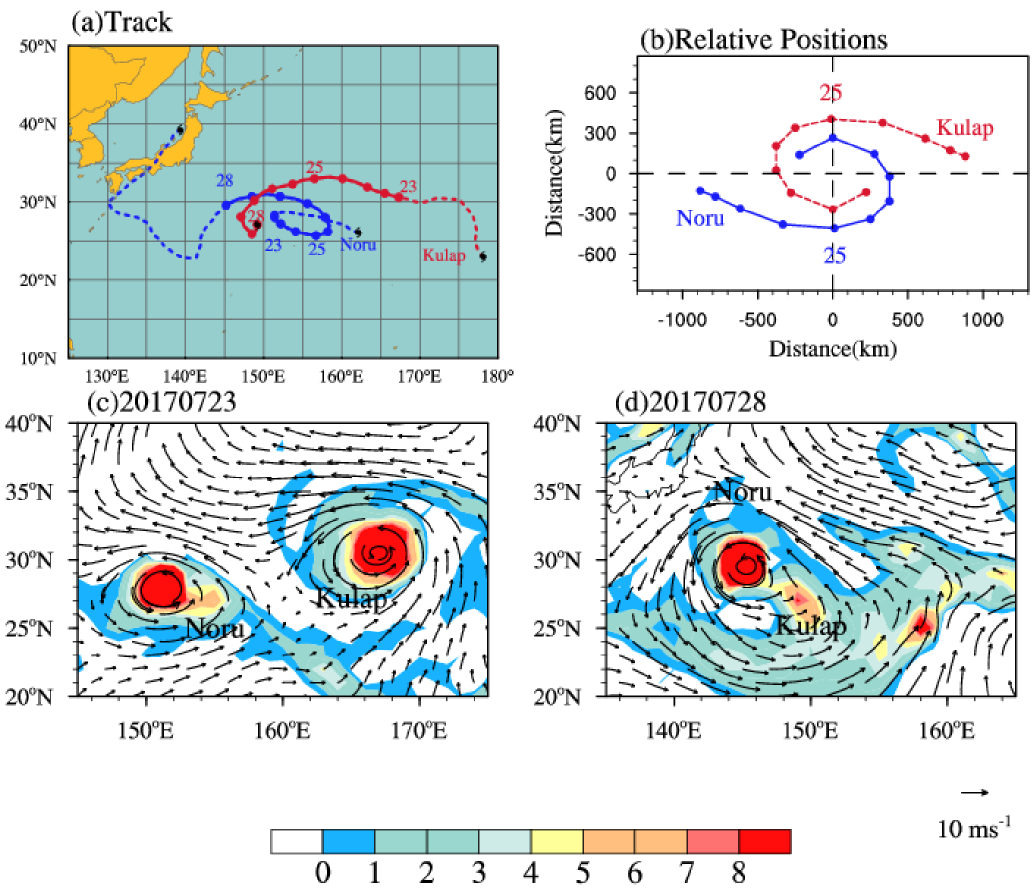

Fig. 1. (a) The JMA 12-hourly best tracks of Noru (blue) and Kulap (red) from 00 UTC 23 July to 00 UTC 28 July 2017. The typhoon symbols denote the beginning and ending of the typhoon positions from the JMA best track data. The dashed line represents the TC's best tracks before it transitions to an extratropical cyclone. The solid line represents the time period of interest in this study; (b) The evolution of relative positions of two TCs. The origin (0, 0) is the middle point between two vortices at each time; (c)-(d) The 850 hPa wind (vector; unit: $\mathrm{m\ s^{-1}}$) and vorticity (shading, unit: $1 \times 10^{-5}\ \mathrm{s^{-1}}$) on 00 UTC 23 July and 00 UTC 28 July 2017.

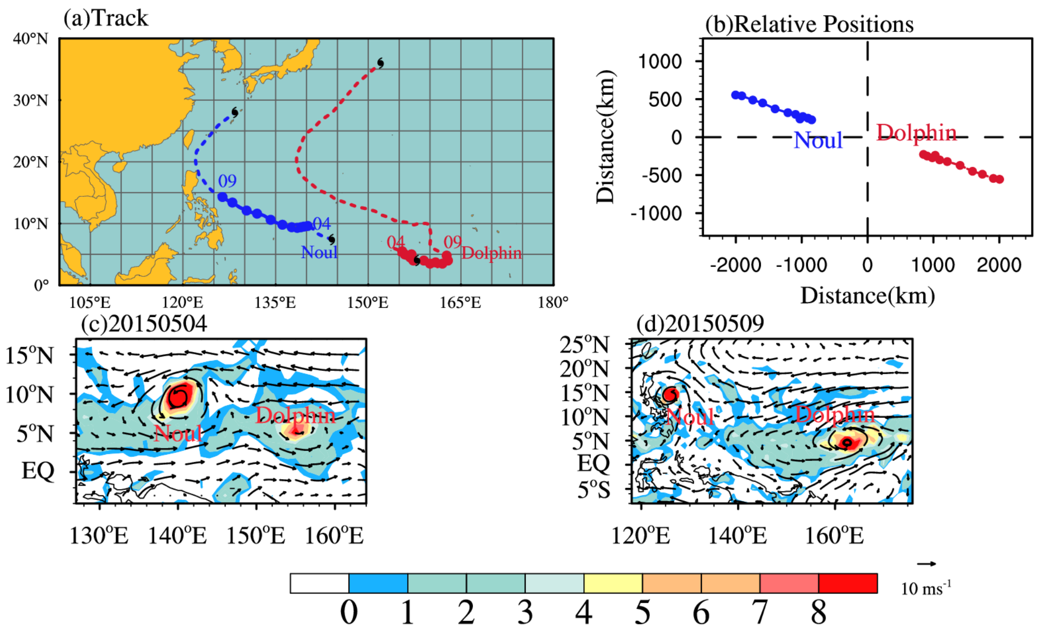

Fig. 2. (a) The 12-hourly track positions of Noul (blue line) and Dolphin (red line) from 00 UTC 4 May to 00 UTC 9 May 2015. The typhoon symbols denote the beginning and ending or the typhoon positions from the JMA best track data. The dashed line represents the TC's best tracks before it transitions to an extratropical cyclone. The solid line represents the time period of interest in this study; (b) The evolution of relative positions of two TCs in which the origin (0,0) is the middle point between two vortices at each time; (c)-(d) The 850 hPa wind (vector; unit: $\mathrm{m\ s^{-1}}$) and vorticity (shading, unit: $1 \times 10^{-5}\ \mathrm{s^{-1}}$) on 00 UTC 4 May and 00 UTC 9 May 2015, respectively.

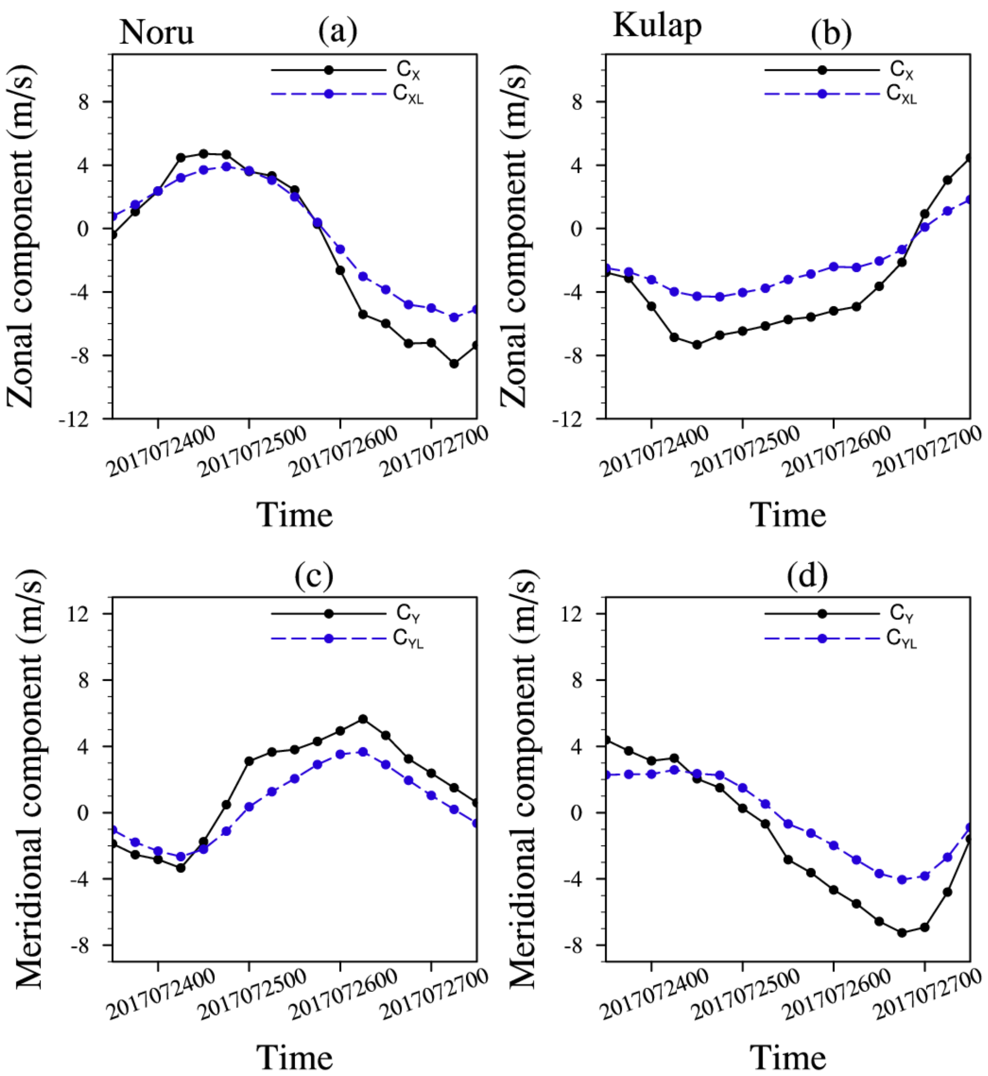

Fig. 3. Evolutions of the steering flows at different scales of the Noru (left panels) and Kulap (right panels). C_X and C_Y (black lines) represent the TC's actual movement speed. C_{XL} and C_{YL} (blue lines) show the large-scale steering flow. X and Y denote the zonal and meridional components, respectively.

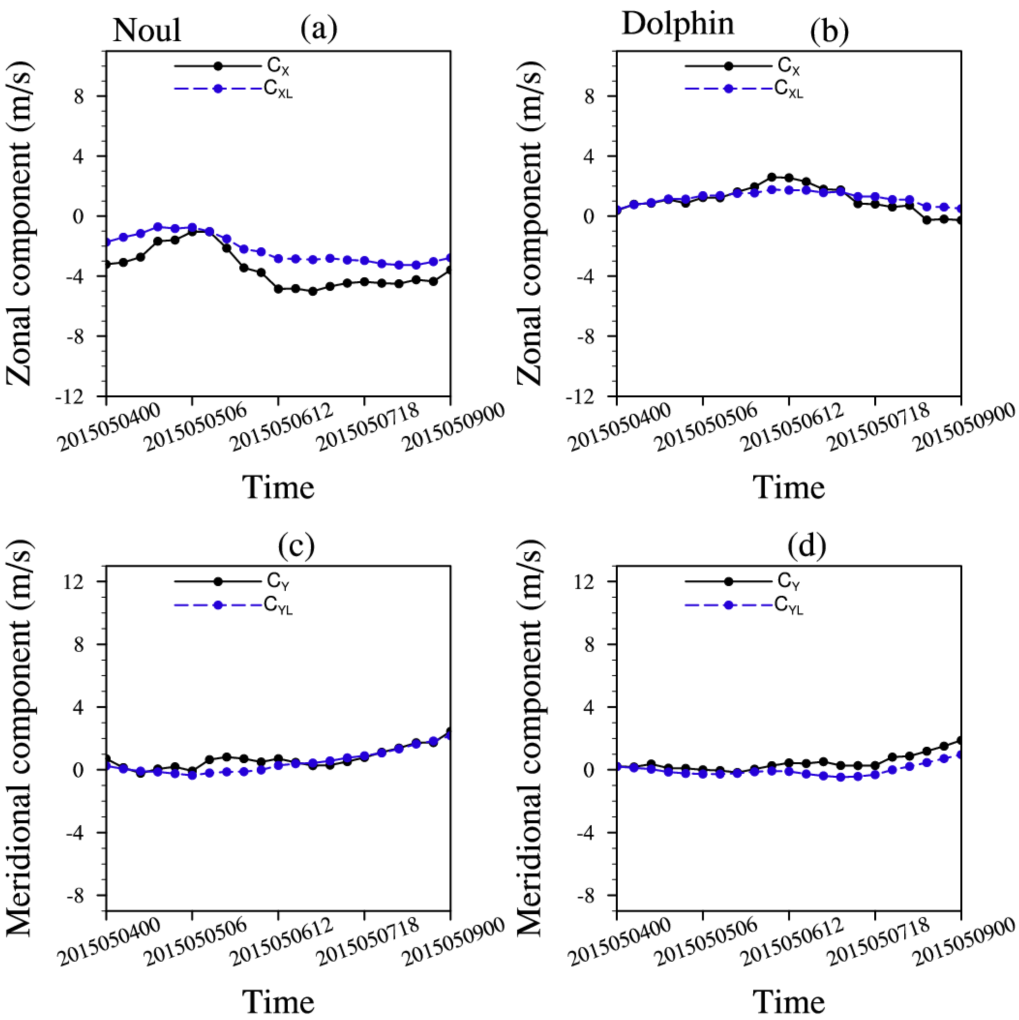

Fig. 4. As in Fig.3, but for Typhoon Noul (left panels) and Dolphin (right panels).

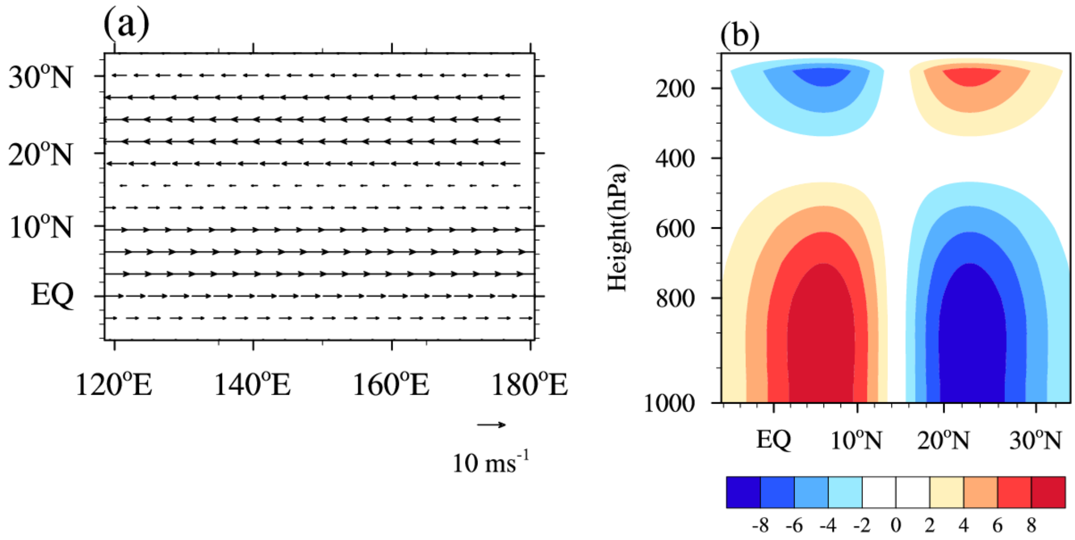

Fig. 5. Initial configurations of (a) 850 hPa wind fields of ideal MT and (b) vertical structure of zonal winds.

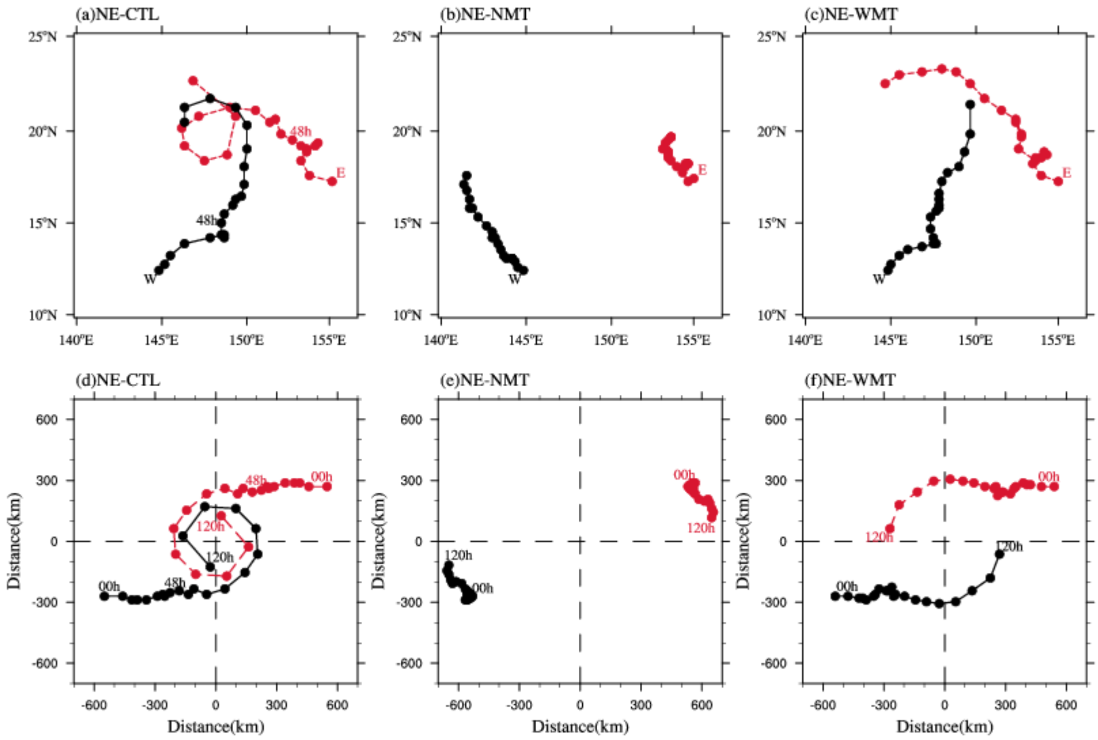

Fig. 6. The tracks (top) and relative positions (bottom) of TCW (black lines) and TCE (red lines) in NE-CTL (left panels), NE-NMT (middle panels), and NE-WMT (right panels) from t = 0 h to 120 h.

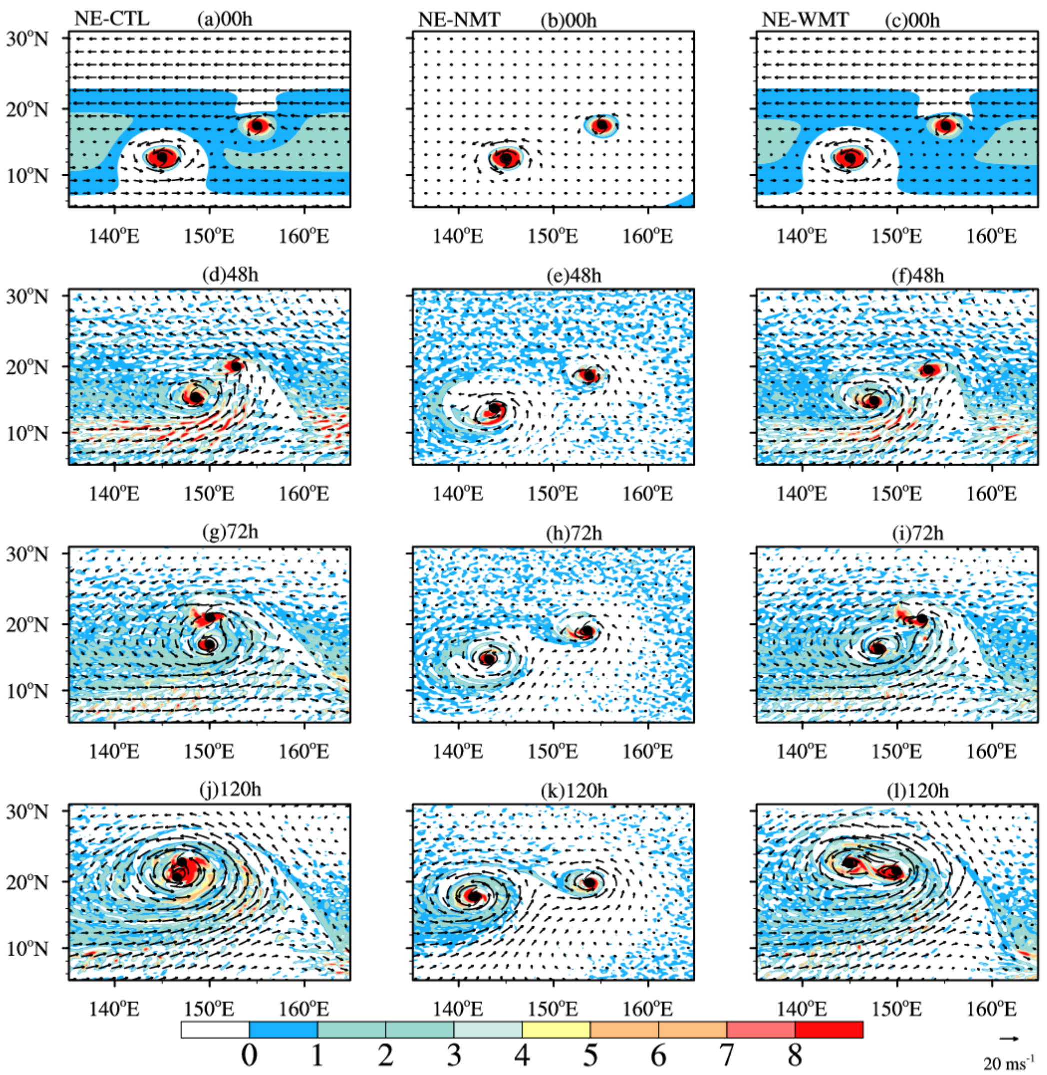

Fig. 7. Time evolutions of 850 hPa wind (vector; unit: $\mathrm{m\ s^{-1}}$) and vorticity (shading; unit: $1 \times 10^{-5}\ \mathrm{s^{-1}}$) in NE-CTL (left panels), NE-NMT (middle panels), and NE-WMT (right panels), respectively.

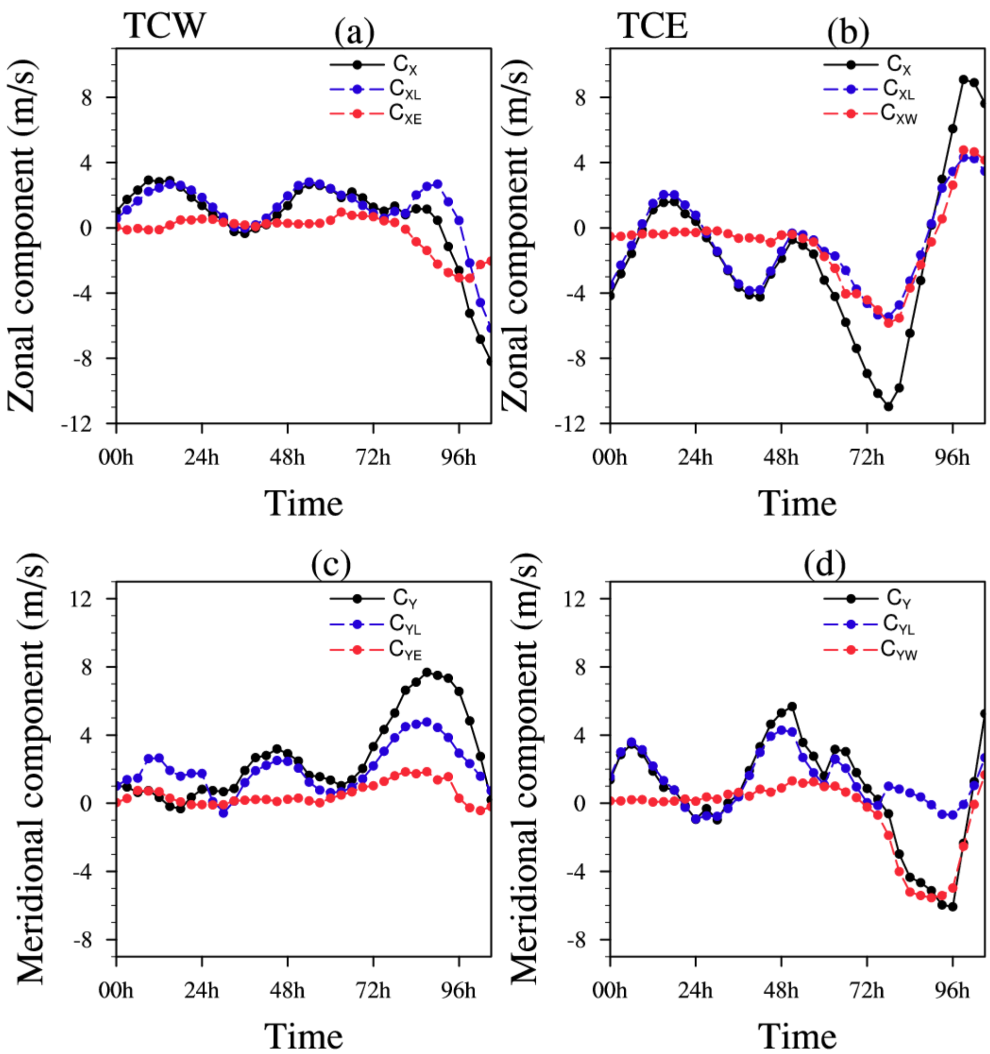

Fig. 8. Evolutions of the steering flows at different scales of the TCW (left panels) and TCE (right panels) in NE-CTL. C_X and C_Y (black lines) represent the actual moving speed of TC.C_{XL} and C_{YL} (blue lines) show the large-scale steering flow. C_{XW}, C_{YW}, C_{XE} and C_{YE} (red lines) present the impact of TCW and TCE on the other storm. X and Y denote the zonal and meridional components, respectively.

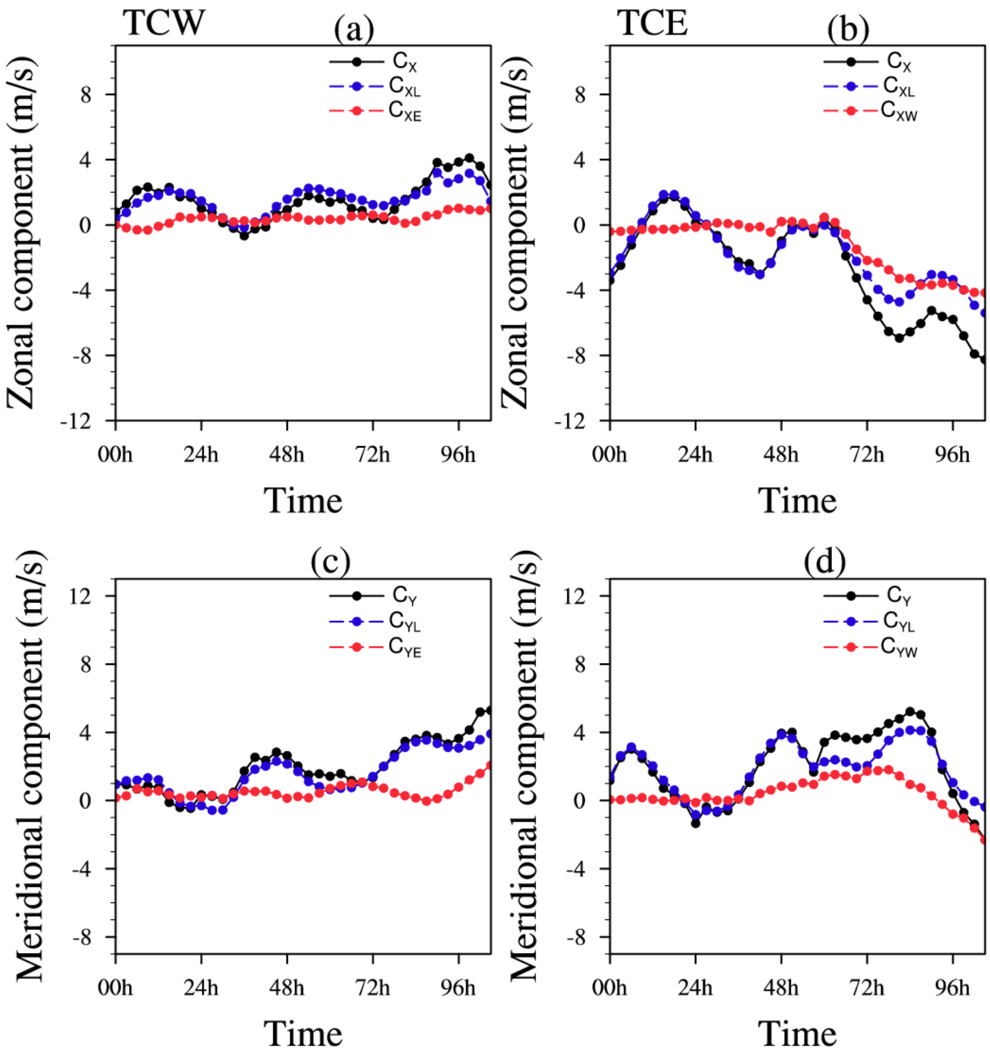

Fig. 9. As in Fig.8, but for NE-WMT.

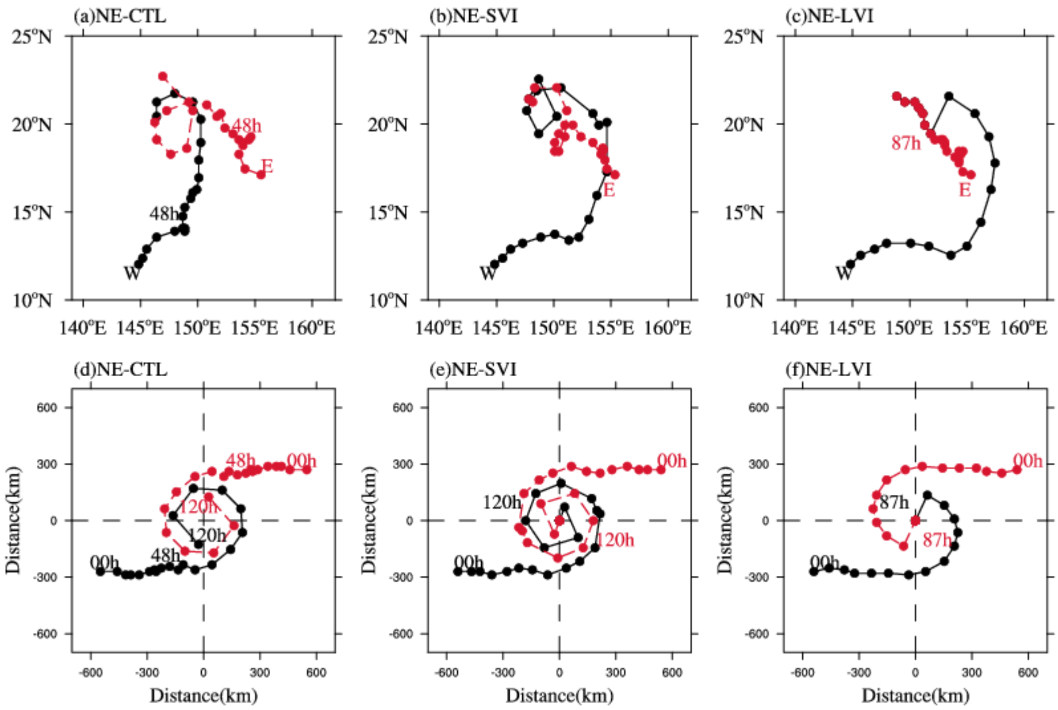

Fig. 10. The tracks (top) and relative positions (bottom) of TCW (black lines) and TCE (red lines) in NE-CTL (left), NE-SVI (middle) and NE-LVI (right) from t = 0 h to 120 h.

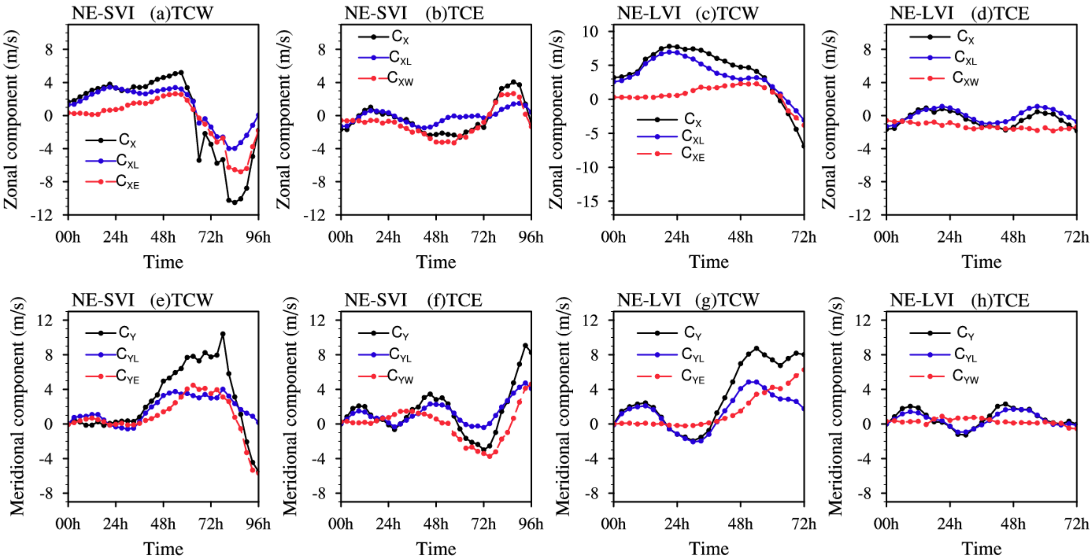

Fig. 11. As in Fig.8, but for NE-SVI (left two panels), and NE-LVI (right two panels).

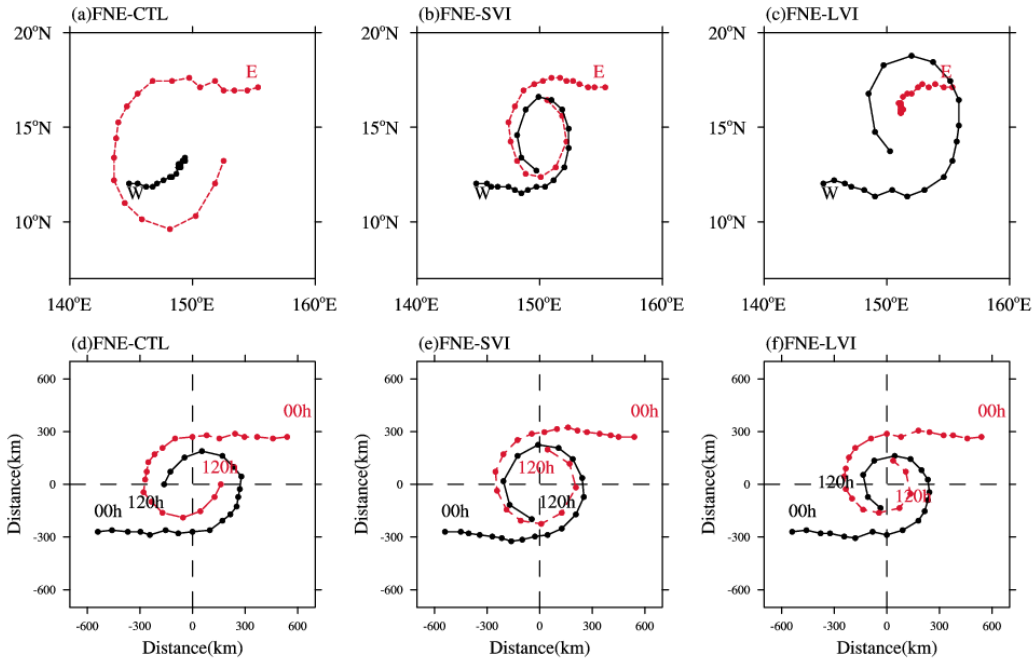

Fig. 12. The tracks (top) and relative positions (bottom) of TCW (black lines) and TCE (red lines) in FNE-CTL (left panels), FNE-SVI (middle panels), and FNE-LVI (right panels) from t = 0 h to 120 h.

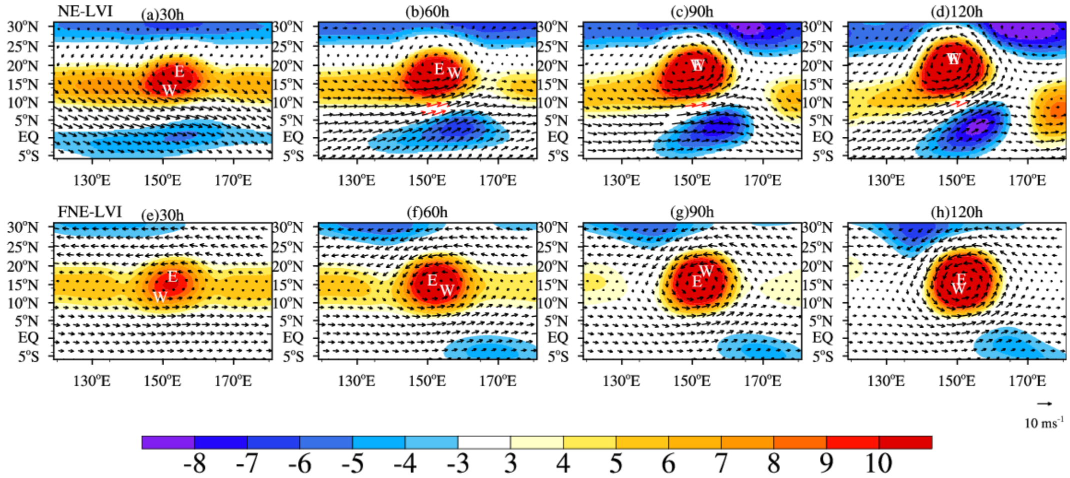

Fig. 13. Evolutions of 850 hPa monsoonal wind (vector; unit: $\mathrm{m\,s^{-1}}$) and vorticity (shading; unit: $1 \times 10^{-6}\ \mathrm{s^{-1}}$) in NE-LVI (top panels) and FNE-LVI (bottom panels). The white "W" and "E" indicate the positions of TCW and TCE correspondingly at that moment. Vectors in red represent wind speeds greater than 10 $\mathrm{m\,s^{-1}}$.

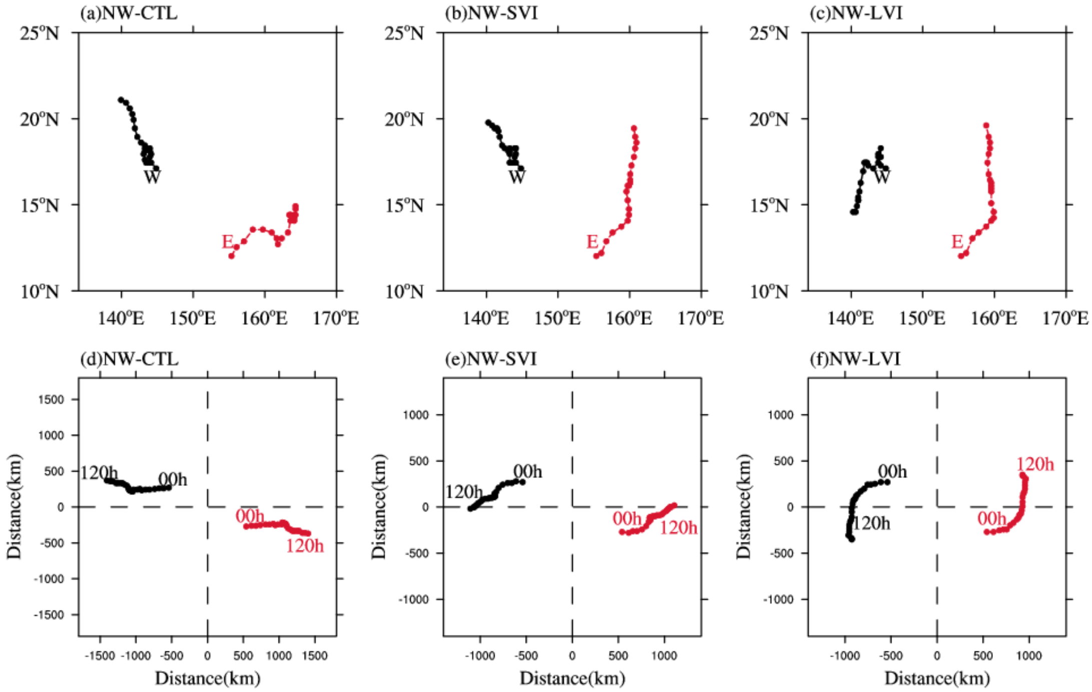

Fig. 14. The tracks (top) and relative positions (bottom) of TCW (black lines) and TCE (red lines) in NW-CTL (left panels), NW-SVI (middle panels), and NW-LVI (right panels) from t = 0 h to 120 h.

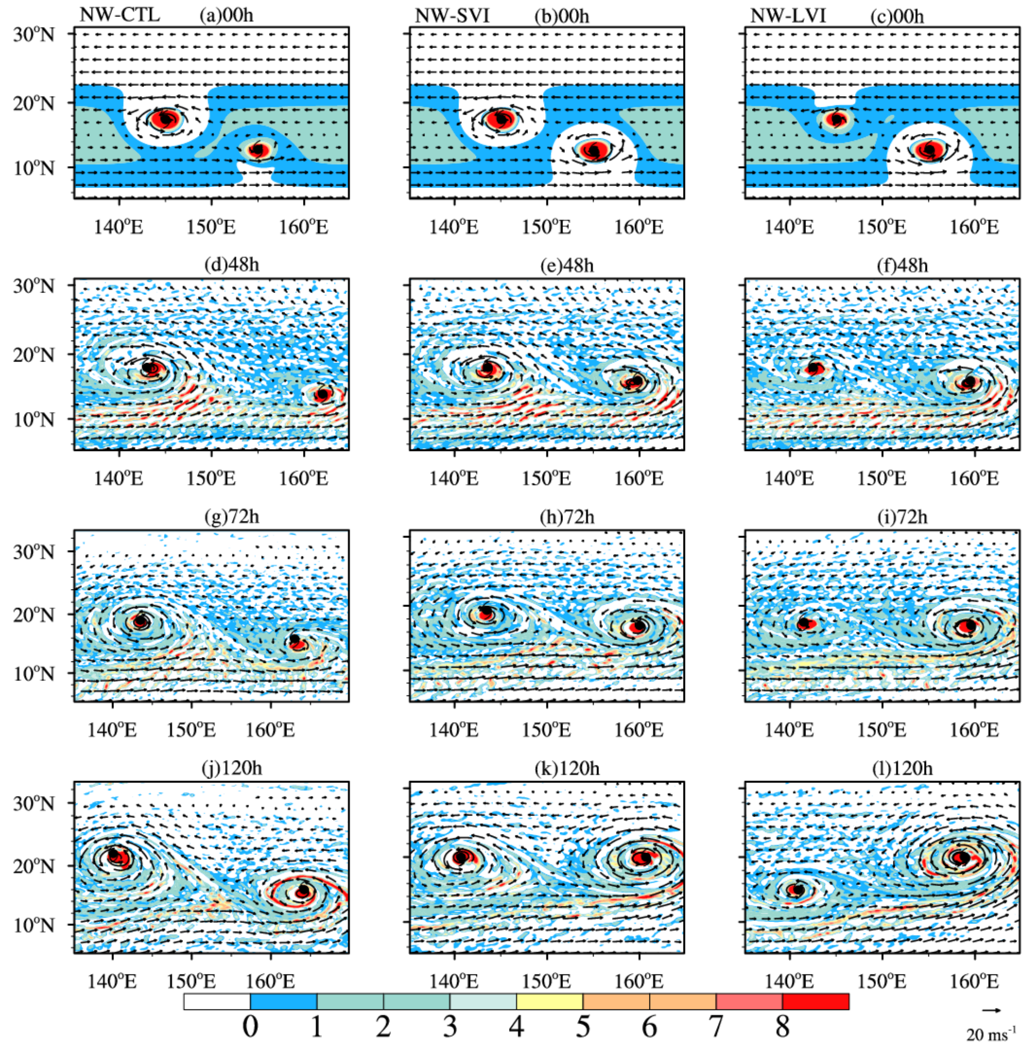

Fig. 15. Time evolutions of 850 hPa wind (vector; unit: $\mathrm{m\ s^{-1}}$) and vorticity (shading; unit: $1 \times 10^{-5}\ \mathrm{s^{-1}}$) in NW-CTL (left panels), NW-SVI (middle panels), and NW-LVI (right panels), respectively.

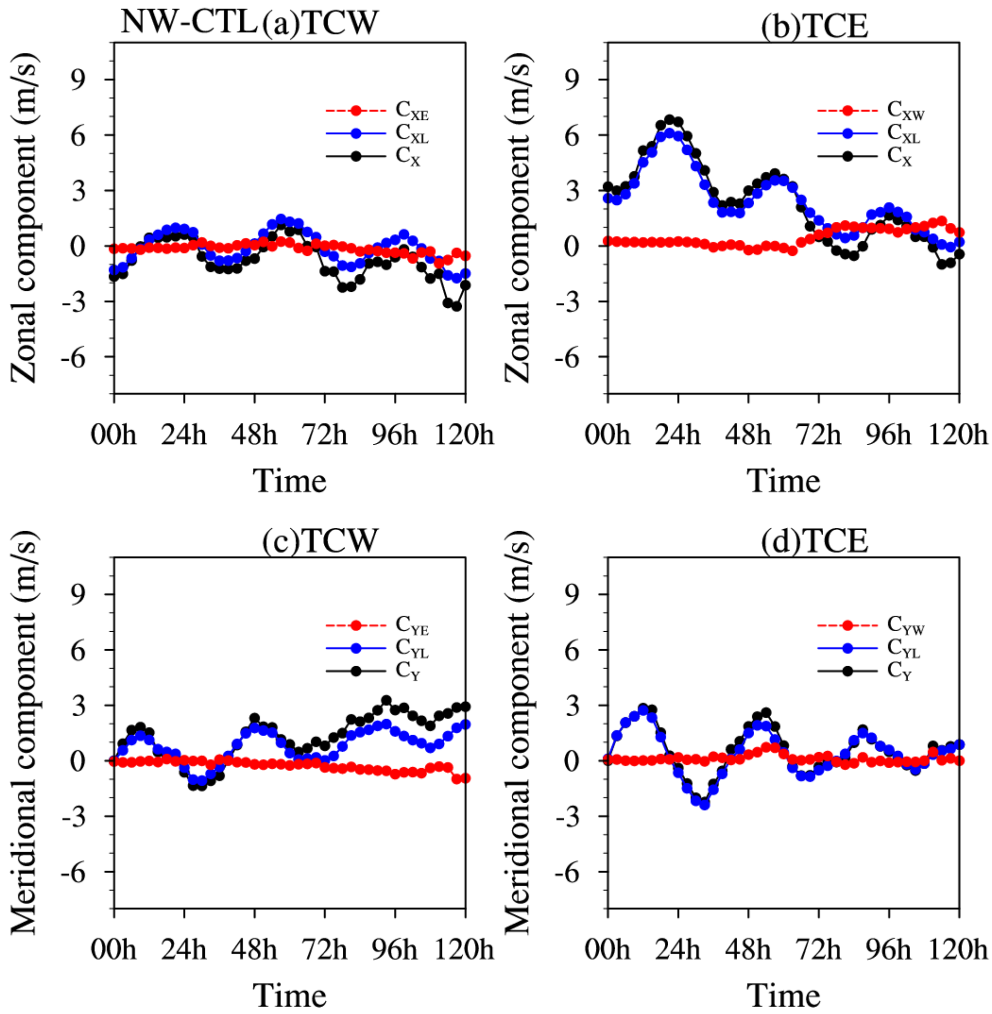

Fig. 16. As in Fig.8, but for NW-CTL.

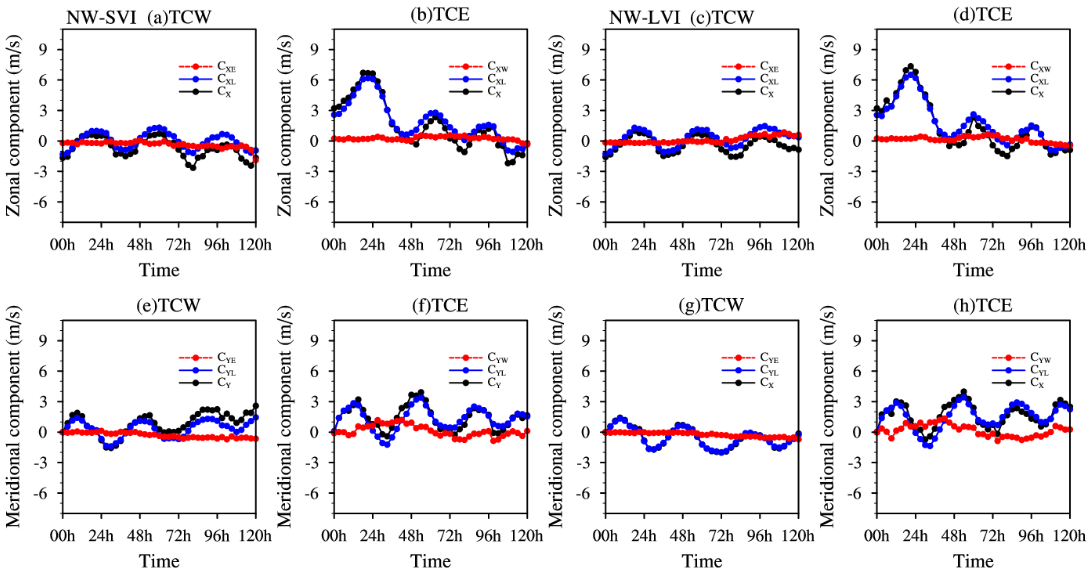

Fig. 17. As in Fig.8, but for NW-SVI (left two panels) and NW-LVI (right two panels).

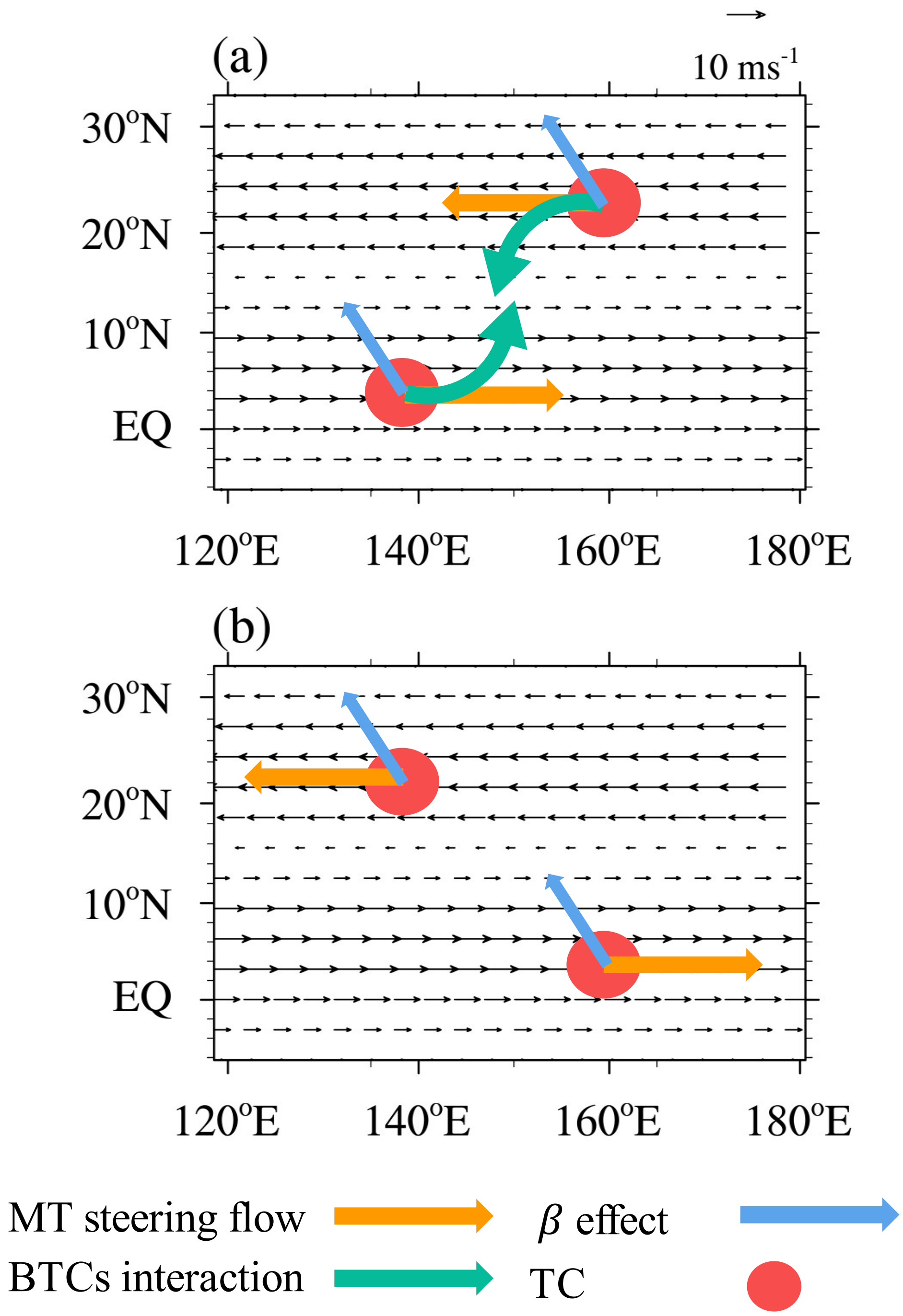

821

822 **Fig. 18.** Conceptual model of the influences of monsoon trough on the BTCs

823 interactions in the (a) NE-SW and (b) NW-SE configuration.